

# Second Order Linear Energy Stable Schemes for Allen-Cahn Equations with Nonlocal Constraints

Xiaobo Jing<sup>1</sup> · Jun Li<sup>1,2</sup> · Xueping Zhao<sup>3</sup> · Qi Wang<sup>1,4,5</sup>

Received: 30 September 2018 / Revised: 14 February 2019 / Accepted: 17 March 2019 / Published online: 5 April 2019

© Springer Science+Business Media, LLC, part of Springer Nature 2019

#### Abstract

We present a set of linear, second order, unconditionally energy stable schemes for the Allen-Cahn equation with nonlocal constraints that preserves the total volume of each phase in a binary material system. The energy quadratization strategy is employed to derive the energy stable semi-discrete numerical algorithms in time. Solvability conditions are then established for the linear systems resulting from the semi-discrete, linear schemes. The fully discrete schemes are obtained afterwards by applying second order finite difference methods on cell-centered grids in space. The performance of the schemes are assessed against two benchmark numerical examples, in which dynamics obtained using the volume-preserving Allen-Cahn equations with nonlocal constraints is compared with those obtained using the classical Allen-Cahn as well as the Cahn-Hilliard model, respectively, demonstrating slower dynamics when volume constraints are imposed as well as their usefulness as alternatives to the Cahn-Hilliard equation in describing phase evolutionary dynamics for immiscible material systems while preserving the phase volumes. Some performance enhancing, practical implementation methods for the linear energy stable schemes are discussed in the end.

 $\textbf{Keywords} \ \ Phase \ field \ model \cdot Energy \ stable \ schemes \cdot Energy \ quadratization \cdot Nonlocal \ constraints \cdot Volume \ preserving$ 

☑ Qi Wang qwang@math.sc.edu

Xiaobo Jing jingxb@csrc.ac.cn

Jun Li nkjunli@foxmail.com

Xueping Zhao xzhao@math.sc.edu

- Beijing Computational Science Research Center, Beijing 100193, P. R. China
- School of Mathematical Sciences, Tianjin Normal University, Tianjin 300387, P. R. China
- Department of Mathematics, University of South Carolina, Columbia, SC 29208, USA
- Department of Mathematics, University of South Carolina, Columbia, SC 29028, USA
- School of Materials Science and Engineering, Nankai University, Tianjin 300350, P. R. China



#### 1 Introduction

Thermodynamically consistent models for material systems represent a class of models that respect the thermodynamical laws and thereby obey the energy dissipation law in isothermal cases. One particular class of the models is known as the gradient flow model, in which the time derivative of thermodynamical variables is proportional to the variation of the system free energy. When the thermodynamic variable is a phase variable, it's known as the Allen-Cahn equation. This class of models describe relaxation dynamics of the thermodynamical system to equilibrium. There are many applications of such gradient flow models, particularly in the materials science, life science and fluid dynamics [1-15]. However, in the case of a phase field description of the Allen-Cahn model, when the phase variable represents the volume fraction of a material component, this model does not warrant the conservation of the volume of that component. In order to preserve the volume, the free energy functional has to be augmented by a volume preserving mechanism with a penalizing potential [16,17] or a Lagrange multiplier [18–20]. This often results in a nonlocal term in the modified Allen-Cahn equation. In this paper, we call these nonlocal Allen-Cahn equations or Allen-Cahn equations with nonlocal constraints. Both methods preserve the volume of each phase at a special definition of the volume. The volume-preserving property of the first method depends on the choice of a suitable penalizing pre-factor, which we will discuss in more details in the paper.

The Cahn–Hilliard equation is an alternative model for the gradient flow model [21,22]. One of its features is its volume preserving property. Rubinstein and Sternberg studied the Allen-Cahn model with a volume constraint analytically and compared it with the Cahn–Hilliard model [18]. Their result seems to be in favor of using the Allen-Cahn model with a volume constraint in place of the Cahn–Hilliard model when studying interfacial dynamics of immiscible multi-component material systems.

For the Allen-Cahn equation as well as the Cahn–Hilliard equation, there have been several popular numerical approaches to construct energy stable schemes for the equations, including the convex splitting approach [12,23–28], the stabilizing approach [29–34], the energy quadratization (EQ) approach [6,8,35,36] and the scalar auxiliary variable (SAV) approach, which is a special form of the EQ strategy [37–40]. Recently, the energy quadratization and the scalar auxiliary variable method have been applied to a host of thermodynamical and hydrodynamic models owing to their simplicity, ease of implementation, computational efficiency, linearity, and most importantly their energy stability property [6,8–11,36,40–46]. This has been an active research area in numerical methods for gradient flow models recently. Interested readers are referred to two review papers on this topic [35,38]. We have shown that the EQ and SAV strategy are general enough to be useful for developing energy stable numerical approximations to any thermodynamically consistent models, i.e., the models derived using the second law of thermodynamics or equivalently the Onsager principle [35, 47,48].

In this paper, we develop a set of linear, second order, unconditionally energy stable schemes using both the energy quadratization (EQ) and the scalar auxiliary variable (SAV) approach to solve the Allen-Cahn equation, nonlocal Allen-Cahn equations and the Cahn-Hilliard equation numerically. The numerical schemes for the Allen-Cahn and the Cahn-Hilliard model are not new. There have been some papers on numerical methods for the model equations cf. [35,37–39]. They are presented here simply for comparison purposes. However, the schemes developed here for the nonlocal Allen-Cahn models are new and useful. In some of these new schemes, both EQ and SAV approaches are combined to yield linear,



energy stable schemes. We note that when a nonlocal Allen-Cahn model is discretized using the EQ strategy in time, it is inevitable to yield a scheme in which an scalar auxiliary variable (SAV) is present due to the volume constraint. When multiple integrals are identified as SAVs in the free energy functional, new iterative procedures are proposed to solve the subproblems in which elliptic equations are solved efficiently using fast solvers. All these schemes we present in this paper are linear and second order accurate in time. The linear system resulting from the schemes are all solvable uniquely so that the solution existence and uniqueness of the semi-discrete linear systems is warranted at least for small time step sizes. When the EQ method is coupled with discretized integrals, the Sherman-Morrison formula can lead us to efficient numerical implementations. This can be equivalently dealt with using the SAV method as well pioneered by Jie Shen et al. [37].

The numerical schemes developed for the Allen-Cahn equation with nonlocal volume-preserving constraints are ensured to preserve the volume of each phase at the discrete level in addition to preserving the energy dissipation rate. To demonstrate the usefulness of the schemes, we conduct two numerical experiments to assess the performance of the schemes. The results based on EQ and those based on SAV perform equally well in preserving the volume and the energy dissipation rate. In addition, the computational efficiency of the schemes is comparatively studied in one of the benchmark examples. Some performance enhancing, practical implementations of the schemes are discussed to improve the accuracy of the schemes at large time step sizes. To simplify our presentation, we present the temporal discretization of the models using EQ and SAV approaches in detail. Then, we briefly discuss our strategy to obtain fully discrete schemes by discretizing the semi-discrete schemes in space on cell centered grids, and refer readers to our early publications in [6,8] for more details.

The rest of paper is organized as follows. In Sect. 2, we present the mathematical models for the Allen-Cahn, the Allen-Cahn with nonlocal constraints, and the Cahn-Hilliard equation. In Sect. 3, we study their near equilibrium dynamics. In Sect. 4, we present a set of second order, linear, energy stable numerical schemes for the models. In Sect. 5, we conduct mesh refinement tests on all the schemes and carry out two simulations on drop merging as well as phase coarsening experiments using the models. Finally, we give the concluding remark in Sect. 6.

# 2 Phase Field Models for Binary Materials

We briefly review two simple phase field models for a binary material system: the Allen-Cahn and the Cahn-Hilliard model, in which the free energy density of the binary material system is given by a functional of phase variable  $\phi \in [0, 1]$  and its gradients. For instance, to study drops of one fluid within the matrix of the other immiscible fluid while ignoring hydrodynamic effects, the free energy is customarily chosen as the following double-well potential:

$$E = \int_{\Omega} \gamma \left[ \frac{\varepsilon}{2} |\nabla \phi|^2 + \frac{1}{\varepsilon} \phi^2 (1 - \phi)^2 \right] d\mathbf{x}, \tag{2.1}$$

where  $\Omega$  is the material domain,  $\epsilon$  is a parameter describing the width of the interface and  $\gamma$  is the surface tension parameter. In general, the generic form of commonly used free energies is given by



$$E = \int_{\Omega} \left[ \frac{\gamma_1}{2} |\nabla \phi|^2 + f(\phi) \right] d\mathbf{x}, \tag{2.2}$$

where  $\gamma_1$  parametrizes the conformational entropy and  $f(\phi)$  is the bulk potential. We denote the free energy density as  $f_d = \frac{\gamma_1}{2} |\nabla \phi|^2 + f(\phi)$ .

Dynamics of the binary material system is customarily governed by a time dependent partial differential equation model resulting from the Onsager's linear response theory [47, 48],

$$\begin{split} \frac{\partial \Phi}{\partial t} &= -M\mu, \quad in \ \Omega, \\ \mu &= \frac{\delta E}{\delta \Phi} = -\gamma_1 \nabla^2 \Phi + f'(\Phi), \end{split} \tag{2.3}$$

subject to appropriate boundary and initial conditions, where M is the mobility matrix consisting of spatial differential operators of even order and  $\mu$  is the chemical potential.

The time rate of change of the free energy, known as the energy dissipation rate functional, is given by

$$\frac{dE}{dt} = -\int_{\Omega} \mu M \mu d\mathbf{x} + \int_{\partial \Omega} \mathbf{n} \cdot \frac{\partial f_d}{\partial \nabla \phi} \phi_t ds. \tag{2.4}$$

The no-flux boundary condition

$$\mathbf{n} \cdot \frac{\partial f_d}{\partial \nabla \phi} = -\gamma_1 \mathbf{n} \cdot \nabla \phi = 0 \tag{2.5}$$

annihilates the energy flux across the boundary, where  $\bf n$  is the unit external normal of the boundary. This is the commonly used boundary condition. Another less-used boundary condition is

$$\phi(\mathbf{x}, t)|_{\partial\Omega} = \phi(\mathbf{x}, 0)|_{\partial\Omega}. \tag{2.6}$$

This boundary condition also annihilates the energy flux across the boundary. A dynamic boundary condition named generalized Navier slip boundary has been used in contact line problems [49,50]

$$\phi_t = -\beta \mathbf{n} \cdot \frac{\partial f_d}{\partial \nabla \phi}. \tag{2.7}$$

This specifies a decay rate of the phase variable at the boundary for  $\beta \geq 0$ , resulting an energy loss at the boundary due to the exchange with the surrounding.

The phase field model equation system is dissipative with respect to all three boundary conditions provided M is a positive definite operator. The commonly used phase field models such as Allen-Cahn and Cahn–Hilliard are two special cases, where M is a prescribed mobility coefficient, which can be a function of  $\phi$ . However, in some cases, a constant mobility is used as an approximation instead. The Allen-Cahn equation defined this way does not conserve the volume defined by  $\int_{\Omega} \phi dx$  if  $\phi$  is the volume-fraction while the Cahn–Hilliard equation does. However, these two models predict similar near equilibrium dynamics revealed in their linear stability analyses below. On the other hand, the Allen-Cahn equation is an equation of lower spatial derivatives, and presumably costs less when solved numerically. However, in order for the Allen-Cahn equation to be useful in the context where volume of each phase is conserved, one has to impose the volume conservation as a constraint. In the following, we will briefly recall several ways to impose volume conservation to dynamics described by



the Allen-Cahn equation, then discuss how to design efficient and energy stable numerical algorithms for the resulting models.

#### 2.1 Allen-Cahn Model

The Allen-Cahn Eq. [1] with the no-flux Neumann boundary condition and initial condition in a domain  $\Omega$  is given as follows:

$$\frac{\partial \Phi}{\partial t} = -M\mu, \quad \mathbf{x} \in \Omega, t > 0,$$

$$\frac{\partial \Phi}{\partial n} = 0, \quad \mathbf{x} \in \partial\Omega,$$

$$\Phi(\mathbf{x}, t)|_{t=0} = \Phi(\mathbf{x}, 0), \quad \mathbf{x} \in \Omega.$$
(2.8)

The energy dissipation rate of the Allen-Cahn equation is given by (2.4). We denote the volume of  $\Omega$  by

$$V(t) = \int_{\Omega} \phi d\mathbf{x}.$$
 (2.9)

Then,

$$\frac{dV}{dt} = -\int_{\Omega} M\mu d\mathbf{x}.$$
 (2.10)

It is normally nonzero when  $M \neq 0$ , which implies that V(t) is not conserved. One simple fix is to impose the volume constraint V(t) = V(0) and couple it to the Allen-Cahn equation. The resulting model is termed the Allen-Cahn model with nonlocal constraints.

#### 2.2 Allen-Cahn Models with Nonlocal Constraints

In addition to the volume defined above by  $V(t) = \int_{\Omega} \phi(t) d\mathbf{x}$ , we can introduce a more general definition using a function  $h(\phi)$ , which is (i) monotonically increasing for  $\phi \in [0, 1]$   $(h'(\phi) \ge 0)$ , and (ii) h(0) = 0, h(1) = 1 as follows,

$$V(t) = \int_{\Omega} h(\phi) d\mathbf{x}.$$
 (2.11)

We next discuss methods to enforce volume conservation for the Allen-Cahn model. First, we consider the method that minimizes  $(V(t) - V(0))^2$  by penalizing it in the free energy functional.

#### 2.2.1 Allen-Cahn Model with a Penalizing Potential

Here, we augment the free energy with a penalizing potential as follows [16,17]

$$E = \int_{\Omega} \left[ \frac{\gamma_1}{2} |\nabla \phi|^2 + f(\phi) \right] d\mathbf{x} + \frac{\eta}{2} (V(t) - V(0))^2, \tag{2.12}$$

where  $\eta$  is the penalizing parameter, a large positive constant. The transport equation for  $\phi$  is given by the Allen-Cahn equation in (2.8) with the modified chemical potential

$$\tilde{\mu} = \frac{\delta E}{\delta \Phi} = \mu + \sqrt{\eta} \zeta h'(\Phi), \quad \zeta = \sqrt{\eta} (V(t) - V(0)). \tag{2.13}$$



The energy dissipation rate is given by

$$\frac{dE}{dt} = \int_{\Omega} \frac{\delta E}{\delta \phi} \phi_t d\mathbf{x} = -\int_{\Omega} \tilde{\mu}(M\tilde{\mu}) d\mathbf{x}. \tag{2.14}$$

It is negative if  $M \ge 0$ . The modified Allen-Cahn model is approximately volume-conserving depending on the size of penalizing potential. In principle, an appropriate  $\eta > 0$  can make V(t) close to V(0). The choice of  $\eta$  is, however, up to the user.

### 2.2.2 Allen-Cahn Model with a Lagrange Multiplier

To impose the volume conservation in the Allen-Cahn model exactly, we use a Lagrange multiplier L to enforce constraint V(t) - V(0) = 0. This can be accomplished by augmenting a penalty term with a Lagrange multiplier L in the free energy functional [18–20] as follows:

$$\tilde{E} = E - L(V(t) - V_0), \quad E = \int_{\Omega} \left[ \frac{\gamma_1}{2} |\nabla \phi|^2 + f(\phi) \right] d\mathbf{x}. \tag{2.15}$$

The transport equation for  $\phi$  is given by the Allen-Cahn equation in (2.8) with a modified chemical potential  $\tilde{\mu}$ :

$$\tilde{\mu} = \frac{\delta \tilde{E}}{\delta \phi} = \mu - Lh'(\phi), \tag{2.16}$$

where  $\mu = \frac{\delta E}{\delta \phi}$  and V(t) - V(0) = 0 is the imposed volume constraint. Since the volume is conserved,

$$\frac{d}{dt}V(t) = \int_{\Omega} \left[ h'(\phi) \frac{d\phi}{dt} \right] d\mathbf{x} = \int_{\Omega} [h'(\phi) M \tilde{\mu}] d\mathbf{x} = 0.$$
 (2.17)

It yields

$$L = \frac{1}{\int_{\Omega} h'(\phi) M h'(\phi) d\mathbf{x}} \int_{\Omega} [h'(\phi) M \mu] d\mathbf{x}.$$
 (2.18)

The volume conserved Allen-Cahn model is nonlocal because an integral is in the chemical potential as well as in the equation. The choices of  $h(\phi)$  considered in this paper include the following two families.

$$h(\phi) = \phi,$$
  

$$h'(\phi) = \frac{(m+1)(2m+1)}{m} [\phi(1-\phi)]^m, m \text{ is a positive integer.}$$
(2.19)

The energy dissipation rate of the model is again given by (2.14) formally.

#### 2.3 Cahn-Hilliard Model

In the Cahn–Hilliard model [2], the transport equation for  $\phi$  is given by

$$\frac{\partial \Phi}{\partial t} = \nabla \cdot (M \nabla \mu), \quad \mathbf{x} \in \Omega 
\frac{\partial \Phi}{\partial n} = 0, \quad \frac{\partial \mu}{\partial n} = 0, \quad \mathbf{x} \in \partial \Omega 
\Phi|_{t=0} = \Phi(\mathbf{x}, 0).$$
(2.20)

The energy dissipation rate of the Cahn-Hilliard equation is given by

$$\frac{dE}{dt} = \int_{\Omega} \frac{\delta E}{\delta \phi} \phi_t d\mathbf{x} = -\int_{\Omega} (\nabla \mu) M(\nabla \mu) d\mathbf{x} \le 0, \tag{2.21}$$



provided M is nonnegative definite. We next examine near equilibrium dynamics of the Allen-Cahn, the nonlocal Allen-Cahn and the Cahn-Hilliard equation, respectively.

# 3 Near Equilibrium Dynamics

For the Allen-Cahn models, including the nonlocal ones, a constant steady state is given by

$$f'(\phi^{ss}) = 0, (3.1)$$

whereas for the Cahn–Hilliard equation, any constant  $\phi^{ss}$  is a steady state. We conduct the linear stability analysis about the constant steady state in a rectangular domain to demonstrate near equilibrium dynamics of the phase field models presented above. We present the analysis only for the case where the mobility is a constant. Specifically, we perturb the constant steady state  $\phi^{ss}$  of the equations by a small disturbance  $\delta \phi$ ,

$$\phi = \phi^{ss} + \delta\phi \tag{3.2}$$

subject to zero Neumann boundary condition

$$\mathbf{n} \cdot \nabla \Phi = 0. \tag{3.3}$$

For the Allen-Cahn model, substituting Eq. (3.2) into Eq. (2.8) and retaining only the linear terms in  $\delta \phi$ , we obtain the linearized equation

$$\frac{\partial \delta \phi}{\partial t} = -M[-\gamma_1 \nabla^2 \delta \phi + f''(\phi^{ss}) \delta \phi] \tag{3.4}$$

together with the boundary condition

$$\mathbf{n} \cdot \nabla \delta \Phi = 0, \mathbf{x} \in \partial \Omega. \tag{3.5}$$

We solve it using the Fourier series method consistent with the no-flux Neumann boundary condition in domain  $\Omega = [-\pi, \pi]^2$  given by

$$\delta \phi = \sum_{k,l=0}^{\infty} a_{kl}(t) \cos(kx) \cos(ly). \tag{3.6}$$

Then we obtain the following ordinary differential equation system for each single mode in the Fourier coefficients:

$$\dot{a}_{kl}(t) = -Ma_{kl}(t)[\gamma_1(k^2 + l^2) + f''(\phi^{ss})], k, l = 0, \dots, \infty.$$
(3.7)

We note that instability may occur only if  $f''(\phi^{ss}) < 0$  and when  $\gamma_1(k^2 + l^2) + f''(\phi^{ss}) < 0$  for some small k, l. This is a well-known result. We present it here to compare with the result obtained from the nonlocal Allen-Cahn equations next.

For the Allen-Cahn model with a penalizing potential, substituting Eq. (3.2) into the transport equation, we get the linearized equation

$$\frac{\partial \delta \Phi}{\partial t} = -M \left( -\gamma_1 \nabla^2 \delta \Phi + f''(\Phi^{ss}) \delta \Phi \right) 
+ \eta \left[ h''(\Phi^{ss}) \delta \Phi \left( \int_{\Omega} h(\Phi^{ss}) d\mathbf{x} - V(0) \right) + h'(\Phi^{ss}) \int_{\Omega} h'(\Phi^{ss}) \delta \Phi d\mathbf{x} \right] \right). (3.8)$$

We solve it analogously and obtain governing system of equations for the Fourier coefficients:



$$\dot{a}_{kl}(t) = -Ma_{kl}(t) \left[ \gamma_1(k^2 + l^2) + f''(\phi^{ss}) + \eta h''(\phi^{ss}) \left( \int_{\Omega} h(\phi^{ss}) d\mathbf{x} - V(0) \right) + \eta h'(\phi^{ss}) \int_{\Omega} h'(\phi^{ss}) d\mathbf{x} \delta_{k0} \delta_{l0} \right].$$
(3.9)

If  $\gamma_1(k^2+l^2)+f''(\varphi^{ss})+\eta h''(\varphi^{ss})(\int_\Omega h(\varphi^{ss})\mathrm{d}\mathbf{x}-V(0))+\eta\int_\Omega (h'(\varphi^{ss}))^2\mathrm{d}\mathbf{x}\delta_{k0}\delta_{l0}<0$  for some small k,l, instability may occur. Compared with the Allen-Cahn model, this nonlocal Allen-Cahn model introduces a stabilizing mechanism at the zero wave number k=l=0 due to  $\eta\int_\Omega (h'(\varphi^{ss}))^2\mathrm{d}\mathbf{x}>0$ , and a potentially destabilizing mechanism if  $h''(\varphi^{ss})(\int_\Omega h(\varphi^{ss})\mathrm{d}\mathbf{x}-V(0))<0$  and stabilizing mechanism if  $h''(\varphi^{ss})(\int_\Omega h(\varphi^{ss})\mathrm{d}\mathbf{x}-V(0))>0$  at any wave numbers. For the case where  $h(\varphi)=\varphi$ , the only contribution is the stabilizing mechanism at k=l=0. For the other cases  $h''(\varphi)\neq 0$ . So, potentially stabilizing or destabilizing effect can occur unless  $\int_\Omega h(\varphi^{ss})\mathrm{d}\mathbf{x}-V(0)=0$ .

This simple analysis shows that the augmented volume penalization in the free energy in the modified Allen-Cahn model alters the linear stability for the longest wave mode, the zero wave number mode when in the volume constraint  $h(\phi) = \phi$ . In addition, if an alternative definition is employed and the volume constraint is not met at the steady state, an additional stabilizing or destabilizing mechanism can show up in all modes depending on the sign of  $h''(\phi^{ss})(\int_{\Omega} h(\phi^{ss})d\mathbf{x} - V(0))$ .

For the Allen-Cahn model with a Lagrangian multiplier, we denote  $g(\phi) = h'(\phi)M$   $(-\gamma_1 \nabla^2 \phi + f'(\phi^{ss}))$ . Substituting Eq. (3.2) into the transport equation, we get the linearized equation

$$\frac{\partial \delta \Phi}{\partial t} = -M \left[ -\gamma_1 \nabla^2 \delta \Phi + f''(\Phi^{ss}) \delta \Phi - \frac{h''(\Phi^{ss}) \delta \Phi \int_{\Omega} g(\Phi^{ss}) d\mathbf{x}}{\int_{\Omega} [h'(\Phi^{ss})] M [h'(\Phi^{ss})] d\mathbf{x}} \right. \\
\left. - \frac{h'(\Phi^{ss}) \int_{\Omega} g'(\Phi^{ss}) \delta \Phi d\mathbf{x}}{\int_{\Omega} [h'(\Phi^{ss})] M [h'(\Phi^{ss})] d\mathbf{x}} \right. \\
\left. + 2 \frac{h'(\Phi^{ss}) \int_{\Omega} g(\Phi^{ss}) d\mathbf{x}}{\left( \int_{\Omega} [h'(\Phi^{ss})] M [h'(\Phi^{ss})] d\mathbf{x} \right)^2} \int_{\Omega} [h''(\Phi^{ss})] M [h'(\Phi^{ss})] \delta \Phi d\mathbf{x} \right]. \quad (3.10)$$

The dynamic equations for the Fourier coefficients are

$$\begin{split} \dot{a}_{kl}(t) &= -Ma_{kl}(t) \left[ \gamma_1(k^2 + l^2) + f''(\phi^{ss}) - \frac{h''(\phi^{ss}) f'(\phi^{ss})}{h'(\phi^{ss})} \right. \\ & \left. - (f''(\phi^{ss}) - \frac{h''(\phi^{ss}) f'(\phi^{ss})}{h'(\phi^{ss})}) \delta_{k0} \delta_{l0} \right] \\ &= \left\{ \begin{aligned} & -Ma_{kl}(t) [\gamma_1(k^2 + l^2)], & k = l = 0, \\ & -Ma_{kl}(t) \left[ \gamma_1(k^2 + l^2) + f''(\phi^{ss}) - \frac{h''(\phi^{ss}) f'(\phi^{ss})}{h'(\phi^{ss})} \right], & \text{otherwise.} \end{aligned} \right. \end{split}$$
(3.11)

For the simple case  $h(\phi) = \phi$ , the equations reduce to

$$\dot{a}_{kl}(t) = -Ma_{kl}(t)[\gamma_1(k^2 + l^2) + f''(\phi^{ss}) - f''(\phi^{ss})\delta_{k0}\delta_{l0}]. \tag{3.12}$$

If  $\gamma_1(k^2+l^2)+(f''(\phi^{ss})-\frac{h''(\phi^{ss})f'(\phi^{ss})}{h'(\phi^{ss})})(1-\delta_{k0}\delta_{l0})<0$ , for small k,l, instability may occur. Compared with the Allen-Cahn model, the only contribution of the Lagrange multiplier is to make the zeroth mode neutrally stable. For the other cases, it is stabilizing if h''f'<0 and destabilizing otherwise. For example, if  $h'(\phi)=\frac{(m+1)(2m+1)}{m}(\phi(1-\phi))^m$  and  $f(\phi)=\gamma_2\phi^2(1-\phi)^2,h''f'>0$ . So, the augmented term is destabilizing.



For the Cahn–Hilliard model, substituting Eq. (3.2) into Eq. (2.20), we get the linearized equation

$$\frac{\partial \delta \Phi}{\partial t} = M[-\gamma_1 \nabla^4 \delta \Phi + f''(\Phi^{ss}) \nabla^2 \delta \Phi)]. \tag{3.13}$$

Repeating the analysis, we have

$$\dot{a}_{kl}(t) = -Ma_{kl}(t)[\gamma_1(k^2 + l^2) + f''(\phi^{ss})](k^2 + l^2). \tag{3.14}$$

If  $\gamma_1(k^2+l^2)+f''(\varphi^{ss})<0$ , instability may ensure. We note that the window of instability in the Cahn–Hilliard model is identical to that in the Allen-Cahn model. However, the rate of growth is different. These linear stability results dictate the initial transition of the solution towards or away from the constant steady state. Both modified nonlocal Allen-Cahn equations carry additional stabilizing or destabilizing mechanisms depending on the base steady state. For long time transient behavior of the solution, we have to resort to numerical computations.

We next discuss how to numerically approximate the model equations efficiently with high order, linear, energy stable schemes.

# 4 Numerical Approximations of the Phase Field Models

We next design numerical algorithms to solve the above equations to ensure that the energy dissipation property of all models as well as the total volume conservation of the modified models are respected, employing the energy quadratization strategy (EQ) and the scalar auxiliary variable approach (SAV) developed recently [10,37,43,44]. These methods require a reformulation of the model into one with a quadratic energy, providing effective ways to design linear and energy stable numerical schemes. For a full review on EQ and SAV methods on thermodynamical systems, readers are referred to recent review articles [35,38].

All schemes presented below are semi-discretized by the Crank-Nilcolson method in time firstly and then fully discretized in space using finite difference methods. In fact, we have shown recently that BDF and Runge-Kutta methods can be used to design energy stable schemes for thermodynamically consistent models up to arbitrarily high order in time [41]. These high order energy stable schemes are normally nonlinear. So, we will not present them in this paper. For simplicity, we present the schemes in their semi-discrete forms in time in detail and discuss briefly the full discretization in space. For comparison purposes, we also present analogous schemes for the classical Allen-Cahn and the Cahn Hilliard model as well, which have been studied before [35,38,39].

#### 4.1 Temporal Discretization

For each model, we present a couple of energy stable schemes derived either using the EQ or the SAV method, and show that they preserve the energy dissipation rate. For the Allen-Cahn model with a Lagrange multiplier, we also prove that derived energy stable schemes also preserve the volume of each phase.



#### 4.1.1 Numerical Methods for the Allen-Cahn Model Using EQ

We reformulate the free energy density by introducing an intermediate variable q, a constant parameter  $\gamma_2 > 0$  and a constant  $C_0 \ge 0$  such that q is a real variable,

$$q = \sqrt{[f(\phi) - \gamma_2 \phi^2 + C_0]}. \tag{4.1}$$

Then, the free energy is recast into a quadratic form:

$$F = \int_{\Omega} \left[ \frac{\gamma_1}{2} |\nabla \phi|^2 + \gamma_2 \phi^2 + q^2 - C_0 \right] d\mathbf{x}. \tag{4.2}$$

The chemical potential is given by

$$\mu = \frac{\delta F}{\delta \Phi} = -\gamma_1 \nabla^2 \Phi + 2\gamma_2 \Phi + 2qq', \quad q' = \frac{\delta q}{\delta \Phi}. \tag{4.3}$$

We rewrite the Allen-Cahn equation given in (2.8) using the new variable q together with a new equation for q as follows

$$\frac{\partial \Phi}{\partial t} = -M\mu,$$

$$\frac{\partial q}{\partial t} = q'\Phi_t.$$
(4.4)

The initial condition of q must be calculated from that of  $\phi$ . We denote

$$(\cdot)^{n+1/2} = \frac{(\cdot)^{n+1} + (\cdot)^n}{2}, \quad \overline{(\cdot)}^{n+1/2} = \frac{3(\cdot)^{n+1} - (\cdot)^n}{2}.$$
 (4.5)

A linear, second order numerical algorithm for model (4.4) is given below.

**Scheme 4.1** Given initial conditions  $\phi^0$  and  $q^0$  (calculated from  $\phi^0$ ), we compute  $\phi^1$ ,  $q^1$  by a first order scheme. Having computed  $\phi^{n-1}$ ,  $q^{n-1}$ , and  $\phi^n$ ,  $q^n$ , we compute  $\phi^{n+1}$ ,  $q^{n+1}$  as follows.

$$\phi^{n+1} - \phi^n = -\delta t \overline{M}^{n+1/2} \mu^{n+1/2}, 
\mu^{n+1/2} = -\gamma_1 \nabla^2 \phi^{n+1/2} + 2\gamma_2 \phi^{n+1/2} + 2q^{n+1/2} \overline{q'}^{n+1/2}, 
q^{n+1} - q^n = \overline{q'}^{n+1/2} (\phi^{n+1} - \phi^n).$$
(4.6)

We define the discrete energy at  $t_n = n\delta t$  as follows

$$F^{n} = \int_{\Omega} \left[ \frac{\gamma_{1}}{2} |\nabla \phi^{n}|^{2} + \gamma_{2} (\phi^{n})^{2} + (q^{n})^{2} - C_{0} \right] d\mathbf{x}. \tag{4.7}$$

The numerical implementation of the algorithm is done in the following steps:

$$\left(\mathbf{I} + \delta t \overline{M}^{n+1/2} \left[ -\frac{\gamma_1}{2} \nabla^2 + \gamma_2 \mathbf{I} + (\overline{q'}^{n+1/2})^2 \right] \right) \phi^{n+1} = b^n, 
b^n = \left( \phi^n - \delta t \overline{M}^{n+1/2} \left[ -\frac{\gamma_1}{2} \nabla^2 \phi^n + \gamma_2 \phi^n + 2q^n \overline{q'}^{n+1/2} - (\overline{q'}^{n+1/2})^2 \phi^n \right] \right),$$

$$(4.8)$$

$$q^{n+1} = q^n + \overline{q'}^{n+1/2} (\phi^{n+1} - \phi^n).$$

 $\phi^{n+1}$  is solved firstly and then  $q^{n+1}$  is updated subsequently. So, the equation of  $\phi^{n+1}$  decouples from the equation of  $q^{n+1}$ .



# 4.1.2 Numerical Method for the Allen-Cahn Model Using SAV

The scalar auxiliary variable (SAV) method provides yet another energy quadratization approach to arrive at linear numerical schemes. We define  $E_1(\phi) = \int_{\Omega} [f(\phi) - \gamma_2 \phi^2] d\mathbf{x}$  and choose a constant  $C_0$  such that  $E_1(\phi) \geq -C_0$ . Setting  $U = \frac{\delta E_1}{\delta \phi}$ , and introducing  $r = \sqrt{E_1 + C_0}$  as the scalar auxiliary variable, we reformulate the free energy as follows

$$F = \int_{\Omega} \left[ \frac{\gamma_1}{2} |\nabla \phi|^2 + \gamma_2 \phi^2 \right] d\mathbf{x} + r^2 - C_0. \tag{4.9}$$

The Allen-Cahn model in new variables  $(\phi, r)$  is recast into an extended equation system

$$\frac{\partial \Phi}{\partial t} = -M\mu, \quad \mu = -\gamma_1 \nabla^2 \Phi + 2\gamma_2 \Phi + rg, 
\frac{\partial r}{\partial t} = \int_{\Omega} \frac{g}{2} \Phi_t d\mathbf{x}, \quad g = 2\frac{\delta r}{\delta \Phi} = \frac{U}{\sqrt{E_1 + C_0}}.$$
(4.10)

We then design a new linear, second order scheme as follows.

**Scheme 4.2** Given initial conditions  $\phi^0$  and  $r^0$ , we compute  $\phi^1$  and  $r^1$  by a first order scheme. Having computed  $\phi^{n-1}$ ,  $r^{n-1}$ ,  $\phi^n$  and  $r^n$ , we compute  $\phi^{n+1}$ ,  $r^{n+1}$  as follows.

$$\phi^{n+1} - \phi^{n} = -\delta t \overline{M}^{n+1/2} \mu^{n+1/2}, 
\mu^{n+1/2} = (-\gamma_{1} \nabla^{2} \phi + 2\gamma_{2} \phi)^{n+1/2} + r^{n+1/2} \overline{g}^{n+1/2}, 
r^{n+1} - r^{n} = \int_{\Omega} \frac{\overline{g}^{n+1/2}}{2} (\phi^{n+1} - \phi^{n}) d\mathbf{x}, \quad \overline{g}^{n+1/2} = \overline{\left(\frac{U(\phi)}{\sqrt{E_{1}(\phi) + C_{0}}}\right)^{n+1/2}}.$$
(4.11)

We define the discrete energy at  $t_n = n\delta t$  as follows

$$F^{n} = \int_{\Omega} \left[ \frac{\gamma_{1}}{2} |\nabla \phi^{n}|^{2} + \gamma_{2} (\phi^{n})^{2} \right] d\mathbf{x} + (r^{n})^{2} - C_{0}.$$
 (4.12)

We next examine how to implement the scheme efficiently. The SAV scheme at the nth time step can be written into the following form

$$A\phi^{n+1} + (c^n, \phi^{n+1})d^n = b^n, \tag{4.13}$$

where

$$A = \mathbf{I} - \delta t \overline{M}^{n+1/2} \left( \frac{\gamma_1}{2} \Delta - \gamma_2 \mathbf{I} \right),$$

$$c^n = \overline{g}^{n+1/2}, \quad d^n = \frac{\delta t \overline{M}^{n+1/2}}{4} \overline{g}^{n+1/2},$$

$$b^n = \phi^n - \delta t \overline{M}^{n+1/2} \left( -\frac{\gamma_1}{2} \Delta \phi^n + \gamma_2 \phi^n + r^n c^n \right) + d^n(c^n, \phi^n),$$

$$(c^n, \phi) = \int_{\Omega} c^n \phi d\mathbf{x}.$$

$$(4.14)$$

This system can be solved efficiently using the following technique. We first multiply (4.13) by  $A^{-1}$  and then take the inner product of the equation with  $c^n$  to obtain

$$(c^n, \phi^{n+1}) + (c^n, \phi^{n+1})(c^n, A^{-1}d^n) = (c^n, A^{-1}b^n). \tag{4.15}$$

It follows that

$$(c^n, \phi^{n+1}) = \frac{(c^n, A^{-1}b^n)}{1 + (c^n, A^{-1}d^n)}.$$
(4.16)

Then, the solution of  $\phi^{n+1}$  and  $r^{n+1}$  are given by

$$\phi^{n+1} = -(c^n, \phi^{n+1}) A^{-1} d^n + A^{-1} b^n, 
r^{n+1} - r^n = \int_{\Omega} \frac{\overline{g}^{n+1/2}}{2} (\phi^{n+1} - \phi^n) d\mathbf{x}.$$
(4.17)



So in each time step, we only need to solve two elliptic equations

$$A[x, y] = [d^n, b^n]. (4.18)$$

The solution in  $(\phi^{n+1}, r^{n+1})$  is then calculated from (4.16) and (4.17). The scheme is decoupled.

#### 4.1.3 Numerical Method for the Allen-Cahn Model with a Penalizing Potential Using EQ

In the Allen-Cahn model with a penalizing potential, we reformulate the free energy density by introducing two intermediate variables

$$q = \sqrt{f(\phi) - \gamma_2 \phi^2 + C_0}, \quad \zeta = \sqrt{\eta} \left( \int_{\Omega} h(\phi(\mathbf{r}, t)) d\mathbf{x} - V_0 \right). \tag{4.19}$$

Then, the free energy is recast into

$$F = \int_{\Omega} \left[ \frac{\gamma_1}{2} |\nabla \phi|^2 + \gamma_2 \phi^2 + q^2 - C_0 \right] d\mathbf{x} + \frac{\zeta^2}{2}.$$
 (4.20)

We rewrite the nonlocal Allen-Cahn equation together with the equations for the new variables as follows:

$$\frac{\partial \Phi}{\partial t} = -M\tilde{\mu}, 
\frac{\partial q}{\partial t} = q'\Phi_t, 
\frac{\partial \xi}{\partial t} = \sqrt{\eta} \int_{\Omega} h'(\Phi) \frac{\partial \Phi}{\partial t} d\mathbf{x}, \tag{4.21}$$

where

$$\tilde{\mu} = -\gamma_1 \nabla^2 \phi + 2\gamma_2 \phi + 2qq' + \zeta \zeta', \quad q' = \frac{\partial q}{\partial \phi}, \quad \zeta' = \frac{\partial \zeta}{\partial \phi} = \sqrt{\eta} h'(\phi). \tag{4.22}$$

We now discretize it using the Crank-Nicolson method to arrive at a new linear, second order scheme as follows.

**Scheme 4.3** Given initial conditions  $\phi^0$ ,  $q^0$ , we compute  $\phi^1$ ,  $q^1$  by a first order scheme. Having computed  $\phi^{n-1}$ ,  $q^{n-1}$ , and  $\phi^n$ ,  $q^n$ , we compute  $\phi^{n+1}$ ,  $q^{n+1}$  as follows.

$$\phi^{n+1} - \phi^{n} = -\delta t \overline{M}^{n+1/2} \tilde{\mu}^{n+1/2}, 
q^{n+1} - q^{n} = \overline{q'}^{n+1/2} (\phi^{n+1} - \phi^{n}), 
\zeta^{n+1} - \zeta^{n} = \sqrt{\eta} \int_{\Omega} \overline{h'}^{n+1/2} (\phi^{n+1} - \phi^{n}) d\mathbf{x}.$$
(4.23)

where

$$\begin{split} \tilde{\mu}^{n+1/2} &= -\gamma_1 \nabla^2 \phi^{n+1/2} + 2\gamma_2 \phi^{n+1/2} + 2q^{n+1/2} \overline{q'}^{n+1/2} + \sqrt{\eta h'}^{n+1/2} \zeta^{n+1/2}, \\ \overline{h'}^{n+1/2} &= h'(\overline{\phi}^{n+1/2}). \end{split} \tag{4.24}$$

We define the discrete energy at  $t_n = n \delta t$  as follows

$$F^{n} = \int_{\Omega} \left[ \frac{\gamma_{1}}{2} |\nabla \phi^{n}|^{2} + \gamma_{2} (\phi^{n})^{2} + (q^{n})^{2} - C_{0} \right] d\mathbf{x} + \frac{(\zeta^{n})^{2}}{2}. \tag{4.25}$$

The new scheme can be recast into

$$A\phi^{n+1} + (\phi^{n+1}, c^n)d^n = b^n, \tag{4.26}$$



where

$$A = \mathbf{I} + \delta t \overline{M}^{n+1/2} \left( -\frac{\gamma_{1}}{2} \nabla^{2} + \gamma_{2} \mathbf{I} + (\overline{q'}^{n+1/2})^{2} \right),$$

$$c^{n} = \overline{h'}^{n+1/2}, d^{n} = \frac{\delta t \overline{M}^{n+1/2} \eta \overline{h'}^{n+1/2}}{2},$$

$$b^{n} = \phi^{n} - \delta t \overline{M}^{n+1/2} \left[ -\frac{\gamma_{1}}{2} \nabla^{2} \phi^{n} + \gamma_{2} \phi^{n} + 2q^{n} \overline{q'}^{n+1/2} - (\overline{q'}^{n+1/2})^{2} \phi^{n} \right]$$

$$-\delta t \overline{M}^{n+1/2} \sqrt{\eta} \overline{h'}^{n+1/2} \zeta^{n} + \frac{\delta t \overline{M}^{n+1/2} \eta}{2} \int_{\Omega} \overline{h'}^{n+1/2} \phi^{n} d\mathbf{x}$$

$$(4.27)$$

We can solve it efficiently in the following steps:

$$A[x, y] = [d^{n}, b^{n}],$$

$$(\phi^{n+1}, c^{n}) = \frac{(y, c^{n})}{1 + (x, c^{n})},$$

$$\phi^{n+1} = -(\phi^{n+1}, c^{n})x + y,$$

$$q^{n+1} = q^{n} + \overline{q}^{n+1/2}(\phi^{n+1} - \phi^{n}),$$

$$\zeta^{n+1} = \zeta^{n} + \sqrt{\eta}((\phi^{n+1} - \phi^{n}), c^{n}).$$

$$(4.28)$$

This is clearly a decoupled scheme. (4.26) can also be solved using the Sherman-Morrison formula to avoid calculating the function with a full rank coefficient matrix (See Appendix-A).

# 4.1.4 Numerical Method for the Allen-Cahn Model with a Penalizing Potential Using SAV

We derive linear schemes for the Allen-Cahn model with a penalizing potential utilizing the SAV approach. We define  $E_1(\phi) = \int_{\Omega} [f(\phi) - \gamma_2 \phi^2] d\mathbf{x}$  and choose a constant  $C_0$  such that  $E_1(\phi) \geq -C_0$ . Setting  $U = \frac{\delta E_1}{\delta \phi}$  and introducing  $r = \sqrt{E_1 + C_0}$  as the scalar auxiliary variable, we arrive at a reformulated free energy as follows.

$$F = \int_{\Omega} \left[ \frac{\gamma_1}{2} |\nabla \phi|^2 + \gamma_2 \phi^2 \right] d\mathbf{x} + \frac{\zeta^2}{2} + r^2 - C_0.$$
 (4.29)

We then present the following linear, second order scheme.

**Scheme 4.4** Given initial conditions  $\phi^0$  and  $r^0$ , we compute  $\phi^1$  and  $r^1$  by a first order scheme. Having computed  $\phi^{n-1}$ ,  $r^{n-1}$ ,  $\phi^n$  and  $r^n$ , we compute  $\phi^{n+1}$ ,  $r^{n+1}$  as follows.

$$\phi^{n+1} - \phi^{n} = -\delta t \overline{M}^{n+1/2} \mu^{n+1/2}, 
\mu^{n+1/2} = (-\gamma_{1} \nabla^{2} \phi + 2\gamma_{2} \phi)^{n+1/2} + r^{n+1/2} \overline{g}^{n+1/2} + \sqrt{\eta} \overline{h'}^{n+1/2} \zeta^{n+1/2}, 
\zeta^{n+1} - \zeta^{n} = \sqrt{\eta} \int_{\Omega} \overline{h'}^{n+1/2} (\phi^{n+1} - \phi^{n}) d\mathbf{x}, 
r^{n+1} - r^{n} = \int_{\Omega} \frac{\overline{g}^{n+1/2}}{2} (\phi^{n+1} - \phi^{n}) d\mathbf{x}, \quad \overline{g}^{n+1/2} = \overline{\left(\frac{U(\phi)}{\sqrt{E_{1}(\phi) + C_{0}}}\right)^{n+1/2}}.$$
(4.30)

We define the discrete energy at  $t_n = n\delta t$  as follows

$$F^{n} = \int_{\Omega} \left[ \frac{\gamma_{1}}{2} |\nabla \phi^{n}|^{2} + \gamma_{2} (\phi^{n})^{2} \right] d\mathbf{x} + \frac{(\zeta^{n})^{2}}{2} + (r^{n})^{2} - C_{0}.$$
 (4.31)

The scheme can be recast into

$$A\phi^{n+1} + (\phi^{n+1}, c_1^n)d_1^n + (\phi^{n+1}, c_2^n)d_2^n = b^n, \tag{4.32}$$



where

$$A = \mathbf{I} + \delta t \overline{M}^{n+1/2} \left( -\frac{\gamma_{1}}{2} \Delta + \gamma_{2} \mathbf{I} \right), c_{1}^{n} = \overline{g}^{n+1/2}, d_{1}^{n} = \frac{\delta t \overline{M}^{n+1/2}}{4} \overline{g}^{n+1/2}, d_{2}^{n} = \frac{\delta t \overline{M}^{n+1/2}}{4} \overline{g}^{n+1/2}, d_{2}^{n} = \frac{\delta t \overline{M}^{n+1/2}}{4} \overline{g}^{n+1/2}, d_{2}^{n} = \frac{\delta t \overline{M}^{n+1/2}}{2} \overline{g}^{n+1/2}, d_{2}^{n} = \frac{\delta t \overline{M}^{n+1/2}}{2} \overline{g}^{n+1/2}, d_{2}^{n} = \frac{\delta t \overline{M}^{n+1/2}}{4} \overline{g}^{n+1/2} \overline{g}^{n+1/2}, d_{2}^{n} = \frac{\delta t \overline{M}^{n+1/2}}{4} \overline{g}^{n+1/2} \overline{g}^{n+1/2}, d_{2}^{n} = \frac{\delta t \overline{M}^{n+1/2}}{4} \overline{g}^{n} = \frac{\delta t \overline{M}^{n+1/2}}{4} \overline{g}^{n+1/2}, d_{2}^{n} = \frac{\delta t \overline{M}^{n+1/2}}{4} \overline{g}^{n} = \frac{\delta t \overline{M}^{n+1/2}}{4} \overline$$

We multiply (4.32) by  $A^{-1}$  and then form inner products with  $c_1$  and  $c_2$ , respectively, to arrive at the following equations:

$$\begin{array}{l} (\varphi^{n+1},\,c_1^n) + (\varphi^{n+1},\,c_1^n)(A^{-1}d_1^n,\,c_1^n) + (\varphi^{n+1},\,c_2^n)(A^{-1}d_2^n,\,c_1^n) = (A^{-1}b^n,\,c_1^n), \\ (\varphi^{n+1},\,c_2^n) + (\varphi^{n+1},\,c_1^n)(A^{-1}d_1^n,\,c_2^n) + (\varphi^{n+1},\,c_2^n)(A^{-1}d_2^n,\,c_2^n) = (A^{-1}b^n,\,c_2^n). \end{array}$$

We solve for  $(\phi^{n+1}, c_1^n)$  and  $(\phi^{n+1}, c_2^n)$  from the above equations after we obtain (x, y, z) from

$$A[x, y, z] = [d_1^n, d_2^n, b^n]. (4.35)$$

Finally, the solution is obtained from the following formula

$$\phi^{n+1} = z - [(\phi^{n+1}, c_1^n)x + (\phi^{n+1}, c_2^n)y], 
r^{n+1} = r^n + (\phi^{n+1} - \phi^n, \frac{\overline{g}^{n+1/2}}{2}), 
\zeta^{n+1} = \zeta^n + \sqrt{\eta}((\phi^{n+1} - \phi^n), c_2^n).$$
(4.36)

The scheme is decoupled and can be implemented efficiently. We remark that (4.34) is solvable provided  $\delta t$  is small enough.

#### 4.1.5 Numerical Method for the Allen-Cahn Model with a Lagrange Multiplier Using EQ

For the Allen-Cahn model with a Lagrange multiplier, we use  $q = \sqrt{f(\phi) - \gamma_2 \phi^2 + C_0}$  to recast the free energy into

$$F = \int_{\Omega} \left[ \frac{\gamma_1}{2} |\nabla \phi|^2 + \gamma_2 \phi^2 + q^2 - C_0 \right] d\mathbf{x}. \tag{4.37}$$

We rewrite (2.8) as

$$\frac{\partial \Phi}{\partial t} = -M\tilde{\mu}, \quad \frac{\partial q}{\partial t} = q'\Phi_t, \tag{4.38}$$

where

$$\tilde{u} = -\gamma_1 \nabla^2 \phi + 2\gamma_2 \phi + 2qq' - h'(\phi)L,$$

$$L = \frac{\int_{\Omega} h'(\phi) M \mu d\mathbf{x}}{\int_{\Omega} h'(\phi) M h'(\phi) d\mathbf{x}}, \quad q' = \frac{\partial q}{\partial \phi}.$$
(4.39)

Discretizing it using the linear Crank-Nicolson method in time, we obtain the following scheme.

**Scheme 4.5** Given initial conditions  $\phi^0$ ,  $q^0$ , we compute  $\phi^1$ ,  $q^1$  by a first order scheme. Having computed  $\phi^{n-1}$ ,  $q^{n-1}$ , and  $\phi^n$ ,  $q^n$ , we compute  $\phi^{n+1}$ ,  $q^{n+1}$  as follows.

where

$$\begin{split} \tilde{\mu}^{n+1/2} &= \left( -\gamma_1 \nabla^2 \phi + 2\gamma_2 \phi \right)^{n+1/2} + 2q^{n+1/2} \overline{q^{n+1/2}} - \overline{h'(\phi)}^{n+1/2} L^{n+1/2}, \\ L^{n+1/2} &= \frac{\int_{\Omega} \overline{h'(\phi)}^{n+1/2} \overline{M}^{n+1/2} \mu^{n+1/2} \mathrm{d}\mathbf{x}}{\int_{\Omega} \overline{h'(\phi)}^{n+1/2} \overline{M}^{n+1/2} \overline{h'(\phi)}^{n+1/2} \mathrm{d}\mathbf{x}}. \end{split} \tag{4.41}$$

Note that  $L^{n+1/2} \neq \frac{L^n + L^{n+1}}{2}$ .

**Theorem 4.1** *Scheme* (4.5) *preserves the volume of each phase in the case of*  $h(\phi) = \phi$ ,

$$\int_{\Omega} h(\phi^{n+1}) d\mathbf{x} = \int_{\Omega} h(\phi^n) d\mathbf{x}.$$
 (4.42)

**Proof** Notice that  $\overline{h'}^{n+1/2} = 1$ . Substituting  $L^{n+1/2}$  into the equation below, we have

$$\int_{\Omega} \frac{h(\phi^{n+1}) - h(\phi^{n})}{\delta t} d\mathbf{x} 
= \int_{\Omega} \overline{h'(\phi)}^{n+1/2} \frac{\phi^{n+1} - \phi^{n}}{\delta t} d\mathbf{x} 
= \int_{\Omega} -\overline{h'(\phi)}^{n+1/2} \overline{M}^{n+1/2} (\mu^{n+1/2} - \overline{h'(\phi)}^{n+1/2} L^{n+1/2}) d\mathbf{x} = 0.$$
(4.43)

It implies that it preserves the volume in the case of  $h(\phi) = \phi$ .

For the other form of  $h(\phi)$ , the theorem can not be proved.

We define the discrete energy under the volume constraint at  $t_n = n\delta t$  as follows

$$F^{n} = \int_{\Omega} \left[ \frac{\gamma_{1}}{2} |\nabla \phi^{n}|^{2} + \gamma_{2} (\phi^{n})^{2} + (q^{n})^{2} - C_{0} \right] d\mathbf{x}.$$
 (4.44)

We can solve the linear system effectively in the following steps:

$$A[x, y, z] = [c^{n}, d^{n}, b^{n}],$$

$$(\phi^{n+1}, c^{n}) = \frac{(z, c^{n})}{1 + (y, c^{n})},$$

$$\phi^{n+1} = z - (\phi^{n+1}, c^{n})x,$$

$$q^{n+1} = q^{n} + \overline{q}^{n+1/2}(\phi^{n+1} - \phi^{n}),$$

$$(4.45)$$

where

$$A = \mathbf{I} + \delta t \overline{M}^{n+1/2} \left( -\frac{\gamma_{1}}{2} \Delta + \gamma_{2} \mathbf{I} + (\overline{q}^{n+1/2})^{2} \right),$$

$$c^{n} = \overline{h'}^{n+1/2} \overline{M}^{n+1/2} \left( -\frac{\gamma_{1}}{2} \Delta + \gamma_{2} \mathbf{I} + (\overline{q'}^{n+1/2})^{2} \right),$$

$$d^{n} = -\frac{\delta t \overline{M}^{n+1/2} \overline{h'}^{n+1/2}}{(\overline{h'}^{n+1/2} \overline{M}^{n+1/2} \overline{h'}^{n+1/2})},$$

$$b^{n} = \phi^{n} - \delta t \overline{M}^{n+1/2} \left( -\frac{\gamma_{1}}{2} \Delta \phi^{n} + \gamma_{2} \phi^{n} + 2q^{n} \overline{q'}^{n+1/2} - (\overline{q'}^{n+1/2})^{2} \phi^{n} \right)$$

$$-(\overline{h'}^{n+1/2} \overline{M}^{n+1/2}, -\frac{\gamma_{1}}{2} \Delta \phi^{n} + \gamma_{2} \phi^{n} + 2q^{n} \overline{q'}^{n+1/2} - (\overline{q'}^{n+1/2})^{2} \phi^{n}) d.$$

$$(4.46)$$

The unknowns  $\phi^{n+1}$  and  $q^{n+1}$  can be solved sequentially. So, this linear scheme is decoupled.



# 4.1.6 Numerical Method for the Allen-Cahn Model with a Lagrange Multiplier Using SAV

We define  $E_1(\phi) = \int_{\Omega} [f(\phi) - \gamma_2 \phi^2] d\mathbf{x}$  and choose a constant  $C_0$  such that  $E_1(\phi) \ge -C_0$ . Setting  $U = \frac{\delta E_1}{\delta \phi}$  and introducing  $r = \sqrt{E_1 + C_0}$  as the scalar auxiliary variable, we rewrite the free energy functional as follows.

$$F = \int_{\Omega} \left[ \frac{\gamma_1}{2} |\nabla \phi|^2 + \gamma_2 \phi^2 \right] d\mathbf{x}$$
$$+ r^2 - C_0 - L \left( \int_{\Omega} h(\phi(\mathbf{x}, t)) d\mathbf{x} - \int_{\Omega} h(\phi(\mathbf{x}, 0)) d\mathbf{x} \right). \tag{4.47}$$

We reformulate the Allen-Cahn model with the volume constraint in the new variables as follows

$$\frac{\partial \Phi}{\partial t} = -M\tilde{\mu}, \quad \frac{\partial r}{\partial t} = r' \Phi_t, \tag{4.48}$$

where

$$\tilde{u} = -\gamma_1 \nabla^2 \phi + 2\gamma_2 \phi + 2rr' - h'(\phi)L, \quad L = \frac{\int_{\Omega} h'(\phi) M \mu d\mathbf{x}}{\int_{\Omega} h'(\phi) M h'(\phi) d\mathbf{x}}, \quad r' = \frac{\delta r}{\delta \phi}. (4.49)$$

From this model, we derive the following linear scheme.

**Scheme 4.6** Given initial conditions  $\phi^0$  and  $r^0$ , we compute  $\phi^1$  and  $r^1$  by a first order scheme. Having computed  $\phi^{n-1}$ ,  $r^{n-1}$ ,  $\phi^n$  and  $r^n$ , we compute  $\phi^{n+1}$ ,  $r^{n+1}$  as follows.

$$\begin{split} & \Phi^{n+1} - \Phi^n = -8t\overline{M}^{n+1/2}\tilde{\mu}^{n+1/2}, \\ & \tilde{\mu}^{n+1/2} = \left( -\gamma_1 \nabla^2 \Phi + 2\gamma_2 \Phi \right)^{n+1/2} + r^{n+1/2}\overline{g}^{n+1/2} - \overline{h'(\Phi)}^{n+1/2}L^{n+1/2}, \\ & L^{n+1/2} = \frac{\int_{\Omega} \overline{h'(\Phi)}^{n+1/2}\overline{M}^{n+1/2} ((-\gamma_1 \nabla^2 \Phi + 2\gamma_2 \Phi)^{n+1/2} + r^{n+1/2}\overline{g}^{n+1/2}) \mathrm{d}\mathbf{x}}{\int_{\Omega} \overline{h'(\Phi)}^{n+1/2}\overline{M}^{n+1/2}\overline{h'(\Phi)}^{n+1/2} \mathrm{d}\mathbf{x}}, \\ & r^{n+1} - r^n = \int_{\Omega} \frac{\overline{g}^{n+1/2}}{2} (\Phi^{n+1} - \Phi^n) \mathrm{d}\mathbf{x}, \quad \overline{g}^{n+1/2} = \overline{\left( \frac{U(\Phi)}{\sqrt{E_1(\Phi) + C_0}} \right)}^{n+1/2}. \end{split}$$

**Theorem 4.2** Scheme (4.6) preserves the volume of each phase in the case of  $h(\phi) = \phi$ ,

$$\int_{\Omega} h(\phi^{n+1}) d\mathbf{x} = \int_{\Omega} h(\phi^n) d\mathbf{x}.$$
 (4.51)

**Proof** The proof is similar to that of Theorem 4.1 and is thus omitted. We define the discrete energy of the model at  $t_n = n\delta t$  as follows

$$F^{n} = \int_{\Omega} \left[ \frac{\gamma_{1}}{2} |\nabla \phi^{n}|^{2} + \gamma_{2} (\phi^{n})^{2} \right] d\mathbf{x} + (r^{n})^{2} - C_{0}.$$
 (4.52)

This scheme can be recast into

$$A\phi^{n+1} + (\phi^{n+1}, c_1^n)d_1^n + (\phi^{n+1}, c_2^n)d_2^n + (\phi^{n+1}, c_1^n)(c_3^n, 1)d_2^n = b^n,$$
 (4.53)

where

$$A = \mathbf{I} + \delta t \overline{M}^{n+1/2} \left( -\frac{\gamma_{1}}{2} \Delta + \gamma_{2} \mathbf{I} \right),$$

$$c_{1}^{n} = \overline{g}^{n+1/2}, d_{1}^{n} = \delta t \overline{M}^{n+1/2} \frac{\overline{g}^{n+1/2}}{4},$$

$$c_{2}^{n} = \overline{h'}^{n+1/2} \overline{M}^{n+1/2} \left( -\frac{\gamma_{1}}{2} \Delta + \gamma_{2} I \right),$$

$$d_{2}^{n} = -\delta t \overline{M}^{n+1/2} \frac{\overline{h'}^{n+1/2}}{\overline{h'}^{n+1/2} \overline{M}^{n+1/2} \overline{h'}^{n+1/2}},$$

$$c_{3}^{n} = \overline{h'}^{n+1/2} \overline{M}^{n+1/2} \frac{\overline{g}^{n+1/2}}{4},$$

$$b^{n} = \phi^{n} - \delta t \overline{M}^{n+1/2} \left( -\frac{\gamma_{1}}{2} \Delta \phi^{n} + \gamma_{2} \phi^{n} + r^{n} \overline{g}^{n+1/2} - \overline{g}^{n+1/2} \int_{\Omega} \frac{\overline{g}^{n+1/2}}{4} \phi^{n} d\mathbf{x} \right)$$

$$-(\overline{h'}^{n+1/2} \overline{M}^{n+1/2}, -\frac{\gamma_{1}}{2} \Delta \phi^{n} + \gamma_{2} \phi^{n} + r^{n} \overline{g}^{n+1/2} - \overline{g}^{n+1/2} \int_{\Omega} \frac{\overline{g}^{n+1/2}}{4} \phi^{n} d\mathbf{x}) d_{2}.$$

$$(4.54)$$

We multiply (4.53) by  $A^{-1}$  and then take the inner product with respect to  $c_1^n$  and  $c_2^n$ , respectively, to obtain the following equations

$$\begin{aligned} &(\varphi^{n+1},\,c_1^n) + (\varphi^{n+1},\,c_1^n)(A^{-1}d_1^n,\,c_1^n) + (\varphi^{n+1},\,c_2^n)(A^{-1}d_2^n,\,c_1^n) \\ &+ (\varphi^{n+1},\,c_1^n)(c_3^n,\,1)(A^{-1}d_2^n,\,c_1^n) = (A^{-1}b^n,\,c_1^n), \\ &(\varphi^{n+1},\,c_2^n) + (\varphi^{n+1},\,c_1^n)(A^{-1}d_1^n,\,c_2^n) + (\varphi^{n+1},\,c_2^n)(A^{-1}d_2^n,\,c_2^n) \\ &+ (\varphi^{n+1},\,c_1^n)(c_3^n,\,1)(A^{-1}d_2^n,\,c_2^n) = (A^{-1}b^n,\,c_2^n). \end{aligned}$$

We solve for  $(\phi^{n+1}, c_1^n)$  and  $(\phi^{n+1}, c_2^n)$  from the above equations after we obtain (x, y, z) from

$$A[x, y, z] = [d_1^n, d_2^n, b^n], \tag{4.56}$$

Finally, the unknowns are calculated from

$$\phi^{n+1} = z - (\phi^{n+1}, c_1^n) x - (\phi^{n+1}, c_2^n) y - (\phi^{n+1}, c_1^n) (c_3^n, 1) y, 
r^{n+1} = r^n + \left(\frac{\overline{g}^{n+1/2}}{2}, (\phi^{n+1} - \phi^n)\right).$$
(4.57)

This is once again a decoupled, linear scheme. In order to make a comparison with the volume preserving Cahn–Hilliard equation for binary material systems, we present two energy stable schemes for the Cahn–Hilliard equation using EQ and SAV method, respectively.

#### 4.1.7 Numerical Methods for the Cahn-Hilliard Model Using EQ

We use  $q = \sqrt{f(\phi) - \gamma_2 \phi^2 + C_0}$  to recast the free energy into

$$F = \int_{\Omega} \left[ \frac{\gamma_1}{2} |\nabla \phi|^2 + \gamma_2 \phi^2 + q^2 - C_0 \right] d\mathbf{x}. \tag{4.58}$$

Then, the chemical potential is given by

$$\mu = \frac{\delta F}{\delta \Phi} = -\gamma_1 \nabla^2 \Phi + 2\gamma_2 \Phi + 2qq', \quad q' = \frac{\partial q}{\partial \Phi}. \tag{4.59}$$

We rewrite (2.20) as

$$\frac{\partial \Phi}{\partial t} = \nabla \cdot (M \nabla \mu), \quad \frac{\partial q}{\partial t} = q' \Phi_t. \tag{4.60}$$

We discretize it using the Crank-Nicolson method to arrive at a second order, linear semidiscrete scheme.



**Scheme 4.7** Given initial conditions  $\phi^0$ ,  $q^0$ , we compute  $\phi^1$ ,  $q^1$  by a first order scheme. Having computed  $\phi^{n-1}$ ,  $q^{n-1}$ , and  $\phi^n$ ,  $q^n$ , we compute  $\phi^{n+1}$ ,  $q^{n+1}$  as follows.

$$\begin{split} & \phi^{n+1} - \phi^n = \delta t \nabla \cdot (\overline{M}^{n+1/2} \nabla \mu^{n+1/2}), \\ & \mu^{n+1/2} = \left( -\gamma_1 \nabla^2 \phi + 2\gamma_2 \phi \right)^{n+1/2} + 2q^{n+1/2} \overline{q'}^{n+1/2}, \\ & q^{n+1} - q^n = \overline{q'}^{n+1/2} (\phi^{n+1} - \phi^n). \end{split} \tag{4.61}$$

We define the discrete energy at  $t_n = n\delta t$  as follows

$$F^{n} = \int_{\Omega} \left[ \frac{\gamma_{1}}{2} |\nabla \phi^{n}|^{2} + \gamma_{2} (\phi^{n})^{2} + (q^{n})^{2} - C_{0} \right] d\mathbf{x}. \tag{4.62}$$

The implementation of the scheme is as follows

$$A \phi^{n+1} = b^{n},$$

$$A = \mathbf{I} - \delta t \nabla \cdot \left( \overline{M}^{n+1/2} \nabla \left[ -\frac{\gamma_{1}}{2} \nabla^{2} + \gamma_{2} \mathbf{I} + (\overline{q'}^{n+1/2})^{2} \right] \right),$$

$$b^{n} = \phi^{n} + \delta t \nabla \cdot \left( \overline{M}^{n+1/2} \nabla \left[ -\frac{\gamma_{1}}{2} \nabla^{2} \phi^{n} + \gamma_{2} \phi^{n} + 2q^{n} \overline{q'}^{n+1/2} - (\overline{q'}^{n+1/2})^{2} \phi^{n} \right] \right),$$

$$q^{n+1} = q^{n} + \overline{q'}^{n+1/2} (\phi^{n+1} - \phi^{n}).$$

$$(4.63)$$

It is a decoupled, linear scheme.

#### 4.1.8 Numerical Methods for the Cahn-Hilliard Model Using SAV

We define  $E_1(\phi) = \int_{\Omega} [f(\phi) - \gamma_2 \phi^2] d\mathbf{x}$  and choose a constant  $C_0$  such that  $E_1(\phi) \ge -C_0$ . Setting  $U = \frac{\delta E_1}{\delta \phi}$ , and introducing  $r = \sqrt{E_1 + C_0}$  as the scalar auxiliary variable, we rewrite the energy functional as follows

$$F = \int_{\Omega} \left[ \frac{\gamma_1}{2} |\nabla \phi|^2 + \gamma_2 \phi^2 \right] d\mathbf{x} + r^2 - C_0. \tag{4.64}$$

In the new variables  $(\phi, r)$ , The Cahn–Hilliard equation is reformulated into

$$\frac{\partial \Phi}{\partial t} = \nabla \cdot (M \nabla \mu), \quad \frac{\partial r}{\partial t} = r' \Phi_t, \tag{4.65}$$

where the chemical potential is given by

$$\mu = \frac{\delta F}{\delta \phi} = -\gamma_1 \nabla^2 \phi + 2\gamma_2 \phi + 2rr', \quad r' = \frac{\delta r}{\delta \phi}.$$
 (4.66)

We obtain a SAV scheme as follows.

**Scheme 4.8** Given initial conditions  $\phi^0$  and  $r^0$ , we compute  $\phi^1$  and  $r^1$  by a first order scheme. Having computed  $\phi^{n-1}$ ,  $r^{n-1}$ ,  $\phi^n$  and  $r^n$ , we compute  $\phi^{n+1}$ ,  $r^{n+1}$  as follows.

$$\phi^{n+1} - \phi^{n} = \delta t \nabla \cdot (\overline{M}^{n+1/2} \nabla \mu^{n+1/2}), 
\mu^{n+1/2} = (-\gamma_{1} \nabla^{2} \phi + 2\gamma_{2} \phi)^{n+1/2} + r^{n+1/2} \overline{g}^{n+1/2}, 
r^{n+1} - r^{n} = \int_{\Omega} \frac{\overline{g}^{n+1/2}}{2} (\phi^{n+1} - \phi^{n}) d\mathbf{x}, \quad \overline{g}^{n+1/2} = \overline{\left(\frac{U(\phi)}{\sqrt{E_{1}(\phi) + C_{0}}}\right)^{n+1/2}}.$$
(4.67)

We define the discrete energy at  $t_n = n\delta t$  as follows

$$F^{n} = \int_{\Omega} \left[ \frac{\gamma_{1}}{2} |\nabla \phi^{n}|^{2} + \gamma_{2} (\phi^{n})^{2} \right] d\mathbf{x} + (r^{n})^{2} - C_{0}.$$
 (4.68)

We can solve it efficiently in the following steps

$$A[x, y] = [d^{n}, b^{n}],$$

$$(\phi^{n+1}, c^{n}) = \frac{(y, c^{n})}{1 + (x, c^{n})},$$

$$\phi^{n+1} = -(\phi^{n+1}, c^{n})x + y,$$

$$r^{n+1} = r^{n} + \int_{\Omega} \frac{\overline{g}^{n+1/2}}{2} (\phi^{n+1} - \phi^{n}) d\mathbf{x},$$

$$(4.69)$$

where

$$A = \mathbf{I} - \delta t (\nabla \overline{M}^{n+1/2} \nabla + \overline{M}^{n+1/2} \Delta) \left( -\frac{\gamma_1}{2} \Delta + \gamma_2 \mathbf{I} \right),$$

$$c^n = \frac{\overline{g}^{n+1/2}}{4}, d^n = -\delta t (\nabla \overline{M}^{n+1/2} \nabla + \overline{M}^{n+1/2} \Delta) \overline{g}^{n+1/2},$$

$$b^n = \phi^n + \delta t (\nabla \overline{M}^{n+1/2} \nabla + \overline{M}^{n+1/2} \Delta)$$

$$\left( \left( -\frac{\gamma_1}{2} \Delta + \gamma_2 \mathbf{I} \right) \phi^n + r^n \overline{g}^{n+1/2} - \overline{g}^{n+1/2} \int_{\Omega} \frac{\overline{g}^{n+1/2}}{4} \phi^n d\mathbf{x} \right).$$

$$(4.70)$$

#### 4.1.9 Energy Dissipation Properties of the Schemes

All the schemes presented above preserve energy dissipation properties of the reformulated models, in which the free energies are quadratized. We summarize the result into one theorem for all schemes. The proof of the energy dissipation property for each scheme is similar, we only prove the theorem for the Allen-Cahn model with a penalizing potential using EQ here and omit others for simplicity.

**Theorem 4.3** Any one of the schemes presented above obeys the following energy dissipation law

$$F^{n+1} - F^{n} = \begin{cases} -\delta t \int_{\Omega} [\tilde{\mu}^{n+1/2} \overline{M}^{n+1/2} \tilde{\mu}^{n+1/2}] d\mathbf{x}, & Allen-Cahn, \\ -\delta t \int_{\Omega} [\nabla \tilde{\mu}^{n+1/2} \cdot \overline{M}^{n+1/2} \cdot \nabla \tilde{\mu}^{n+1/2}] d\mathbf{x}, & Cahn-Hilliard, \end{cases}$$
(4.71)

for any  $\delta t > 0$ , where the free energy is defined respectively in each scheme as a quadratic functional. Hence, they are unconditionally energy stable.

**Proof** We prove the theorem for Scheme (4.23) here. Taking the  $L^2$  inner product of  $\frac{\phi^{n+1}-\phi^n}{\delta t}$  with  $-\tilde{\mu}^{n+1/2}$ , we obtain

$$-\left(\frac{\Phi^{n+1}-\Phi^n}{\delta t}, \tilde{\mu}^{n+1/2}\right) = (\overline{M}^{n+1/2}[\mu^{n+1/2}+\sqrt{\eta}\zeta^{n+1/2}], \mu^{n+1/2}+\sqrt{\eta}\zeta^{n+1/2})$$

$$= \left\|\sqrt{\overline{M}^{n+1/2}}(\mu^{n+1/2}+\sqrt{\eta}\zeta^{n+1/2})\right\|^2,$$
(4.72)



Taking the  $L^2$  inner product of  $\tilde{\mu}^{n+1/2}$  with  $\frac{\phi^{n+1}-\phi^n}{\delta t}$ , we obtain

$$\left( (-\gamma_{1}\nabla^{2}\phi + 2\gamma_{2}\phi)^{n+1/2} + 2q^{n+1/2}\overline{q'}^{n+1/2} + \sqrt{\eta}\zeta^{n+1/2}, \frac{\phi^{n+1} - \phi^{n}}{\delta t} \right) 
= \frac{\gamma_{1}}{2\delta t} (\|\nabla\phi^{n+1}\|^{2} - \|\nabla\phi^{n}\|^{2}) + \frac{\gamma_{2}}{\delta t} (\|\phi^{n+1}\|^{2} - \|\phi^{n}\|^{2}) 
+ \left( 2q^{n+1/2}\overline{q'}^{n+1/2}, \frac{\phi^{n+1} - \phi^{n}}{\delta t} \right) + \left( \sqrt{\eta}\zeta^{n+1/2}, \frac{\phi^{n+1} - \phi^{n}}{\delta t} \right).$$
(4.73)

Taking the  $L^2$  inner product of  $q^{n+1} - q^n$  with  $\frac{q^{n+1} + q^n}{\delta t}$ , we obtain

$$\frac{1}{\delta t}(\|q^{n+1}\|^2 - \|q^n\|^2) = \frac{1}{\delta t}(\overline{q^n}^{n+1/2}(\phi^{n+1} - \phi^n), q^{n+1} + q^n). \tag{4.74}$$

Taking the  $L^2$  inner product of  $\zeta^{n+1} - \zeta^n$  with  $\frac{\zeta^{n+1} + \zeta^n}{\delta t}$ , we obtain

$$\frac{1}{\delta t} (\|\zeta^{n+1}\|^2 - \|\zeta^n\|^2) = \frac{1}{\delta t} \left( \sqrt{\eta} \int_{\Omega} (\phi^{n+1} - \phi^n) d\mathbf{x}, \zeta^{n+1} + \zeta^n \right). \tag{4.75}$$

Combining the above equations, we have

$$\frac{\gamma_{1}}{2\delta t}(\|\nabla \phi^{n+1}\|^{2} - \|\nabla \phi^{n}\|^{2}) + \frac{\gamma_{2}}{\delta t}(\|\phi^{n+1}\|^{2} - \|\phi^{n}\|^{2}) 
+ \frac{1}{\delta t}(\|q^{n+1}\|^{2} - \|q^{n}\|^{2}) + \frac{1}{2\delta t}(\|\zeta^{n+1}\|^{2} - \|\zeta^{n}\|^{2}) 
= - \left\|\sqrt{\overline{M}^{n+1/2}}(\mu^{n+1/2} + \sqrt{\eta}\zeta^{n+1/2})\right\|^{2}.$$
(4.76)

This leads to the energy stability equality.

#### 4.1.10 Solvability of the Linear Systems Resulting from the Schemes

We summarize the property of the unique solvability for all linear systems resulting from the schemes for the Allen-Cahn model and the Allen-Cahn model with a penalizing potential presented above into a theorem. A similar theorem for the Cahn-Hilliard model can be found in [42]. We state another theorem for the linear systems resulting from the schemes for the Allen-Cahn model with a Lagrange multiplier with a constraint on the small time step size.

**Theorem 4.4** Assuming the mobility is a constant, the linear system resulting from any scheme for the Allen-Cahn and nonlocal Allen-Cahn model with a penalizing potential admits a unique weak solution.

**Proof** For simplicity, we assume *M* is a positive constant mobility coefficient. We only present the detailed proof for the scheme of the Allen-Cahn model with a penalizing potential using EQ since the proofs for the other schemes are similar. The scheme for the nonlocal Allen-Cahn model can be generically written into:

$$A\phi^{n+1} + (\phi^{n+1}, c^n)d^n = b^n, \tag{4.77}$$



where  $A = \mathbf{I} + \delta t M (-\frac{\gamma_1}{2}\Delta + \gamma_2 \mathbf{I} + (\overline{q'}^{n+1/2})^2)$ ,  $b^n$  is the given right hand side term,  $c^n = \overline{h'}^{n+1/2}$  and  $d^n = \frac{\delta t M \eta \overline{h'}^{n+1/2}}{2}$ . We rewrite the linear equation into

$$\mathscr{A}\phi^{n+1} = b^n, \tag{4.78}$$

where  $\mathscr{A}$  is a linear spatial operator. To prove the uniqueness of the solution, we need to prove that the linear spatial operator  $\mathscr{A}$  is symmetric and positive definite.

In fact,  $\exists C > 0$  such that

$$(\mathscr{A}\phi, \phi) = (A\phi, \phi) + (\phi, c^n)(d^n, \phi)$$

$$= (A\phi, \phi) + (\phi, c^n)(c^n, \phi) \frac{M\delta t\eta}{2} \geqslant (A\phi, \phi) > C \|\phi\|_{L^2}^2. \tag{4.79}$$

We can easily show that the operator  $\mathscr{A}$  is bounded above by  $\bar{C} \|\phi\|_{L^2}^2$  since  $\|\overline{q''}^{n+1/2}\|_{L^2}^2$  is bounded. The boundedness of  $\|\overline{q''}^{n+1/2}\|_{L^2}^2$  stems from the fact that  $\|q''\|_{L^2}^2$  and  $\|\phi''\|_{L^2}^2$  are bounded obtained from the quadratic energy dissipation law of each model.

Now we define  $\|\phi\|_{\mathscr{A}} = \sqrt{(\mathscr{A}\phi, \phi)}$  for any  $\phi \in L^2_N(\Omega)$  and the subset  $\Phi = \{\phi \in L^2_N(\Omega) : \|\phi\|_{\mathscr{A}} < \infty\}$ , where  $L^2_N(\Omega)$  is a subspace of  $L^2(\Omega)$  satisfying the zero Neumann boundary condition. It is obvious that  $\|\phi\|_{\mathscr{A}}$  is a norm for  $L^2_N(\Omega)$  and  $L^2_N(\Omega)$  is a Hilbert subspace with the norm. Applying the Lax-Milgram theorem, the uniqueness of the solution of the linear systems in  $\Phi$  is established.

**Theorem 4.5** The linear system resulting from any scheme for the Allen-Cahn model with a Lagrange multiplier admits a unique weak solution at a sufficiently small time step size.

**Proof** We first prove the result for the scheme of the Allen-Cahn model with a Lagrange multiplier using EQ. From Scheme (4.40) we understand that in order to prove the uniqueness of the solution of linear system

$$A\phi^{n+1} + (c^n, \phi^{n+1})d^n = b^n \tag{4.80}$$

with the zero Neumann boundary condition, we only need to prove that

$$A\phi^{n+1} + (c^n, \phi^{n+1})d^n = 0 (4.81)$$

has the zero solution only, where A,  $c^n$ ,  $d^n$ ,  $b^n$  are given in (4.46).

It follows from (4.81) that

$$(c^n, \phi^{n+1})(1 + (c^n, A^{-1}d^n)) = 0. (4.82)$$

Notice that  $d^n = -\frac{\delta t \overline{M}^{n+1/2} \overline{h'}^{n+1/2}}{(\overline{h'}^{n+1/2}, \overline{M}^{n+1/2} \overline{h'}^{n+1/2})} < 0.$ 

$$(c^{n}, A^{-1}d^{n}) = -\frac{\delta t}{(\overline{h'}^{n+1/2}, \overline{M}^{n+1/2}\overline{h'}^{n+1/2})}(c^{n}, A^{-1}(\overline{M}^{n+1/2}\overline{h'}^{n+1/2})).$$
(4.83)

So, for sufficiently small  $\delta t > 0$ ,  $1 + (c^n, A^{-1}) > 0$ . It then follows that  $(c^n, \phi^{n+1}) = 0$ , which in turn implies  $\phi^{n+1} = 0$  from  $A\phi^{n+1} = 0$ .

We then prove the result for the scheme derived using SAV. We notice that we need only to prove the uniqueness of the solution for Eq. (4.55). So, we only need to prove the uniqueness of its corresponding homogeneous system

$$B\begin{bmatrix} (\phi^{n+1}, c_1^n) \\ (\phi^{n+1}, c_2^n) \end{bmatrix} = \begin{bmatrix} 0 \\ 0 \end{bmatrix}, \tag{4.84}$$



where 
$$B = \begin{bmatrix} 1 + (A^{-1}d_1^n, c_1^n) + (c_3^n, 1)(A^{-1}d_2^n, c_1^n) & (A^{-1}d_2^n, c_1^n) \\ (A^{-1}d_1^n, c_2^n) + (c_3^n, 1)(A^{-1}d_2^n, c_2^n) & 1 + (A^{-1}d_2^n, c_2^n) \end{bmatrix}$$
.

$$det(B) = 1 + (A^{-1}d_1^n, c_1^n) + ((c_3^n, 1) - (A^{-1}d_1^n, c_2^n))(A^{-1}d_2^n, c_1^n)$$

$$+ (A^{-1}d_2^n, c_2^n)(1 + (A^{-1}d_1^n, c_1^n)).$$

$$(4.85)$$

Notice that  $d_1^n=\delta t\,\overline{M}^{n+1/2}\frac{\overline{g}^{n+1/2}}{4}, d_2^n=-\delta t\,\overline{M}^{n+1/2}\frac{\overline{h'}^{n+1/2}}{(\overline{h'}^{n+1/2},\overline{M}^{n+1/2}\overline{h'}^{n+1/2})}.$  For sufficiently small  $\delta t>0, det(B)\neq 0$ , which implies  $(\varphi^{n+1},c_1^n)=0, (\varphi^{n+1},c_2^n)=0.$  Then,  $A\varphi^{n+1}=0$  implies  $\varphi^{n+1}=0.$  This completes the proof.

#### 4.2 Spatial Discretization

We use the finite difference method to discretize the semidiscrete schemes presented above in space. The Neumann boundary condition is adopted in the discretization. We divide the 2D domain  $\Omega = [0, L_x] \times [0, L_y]$  into uniform rectangular meshes with mesh sizes  $h_x = L_x/N_x$  and  $h_y = L_y/N_y$ , where  $L_x$ ,  $L_y$  are two positive real numbers and  $N_x$ ,  $N_y$  are the number of meshes in the x and y direction, respectively. The sets of the cell center points  $C_x$  and  $C_y$  in the uniform partition are defined as follows

$$C_x = \{x_i | i = 0, 1, ..., N_x\},\$$
  
 $C_y = \{y_j | j = 0, 1, ..., N_y\},\$ 

$$(4.86)$$

where  $x_i = (i - \frac{1}{2})h_x$  and  $y_j = (j - \frac{1}{2})h_y$ . The phase field variable is discretized at the cell center points  $C_x \times C_y$ .

We define the east-west-edge-to-center and center-to-east-west-edge difference operators  $d_x$  and  $D_x$ , respectively,

$$d_x \phi_{ij} = \frac{\phi_{i+\frac{1}{2},j} - \phi_{i-\frac{1}{2},j}}{h_x}, \qquad D_x \phi_{i+\frac{1}{2},j} = \frac{\phi_{i+1,j} - \phi_{i-1,j}}{h_x}. \tag{4.87}$$

Similarly, we can get the north-south-edge-to-center and center-to-north-south-edge difference operators  $d_v$  and  $D_v$ , respectively,

$$d_{y}\phi_{ij} = \frac{\phi_{i,j+\frac{1}{2}} - \phi_{i,j-\frac{1}{2}}}{h_{y}}, \qquad D_{y}\phi_{i,j+\frac{1}{2}} = \frac{\phi_{i,j+1} - \phi_{i,j-1}}{h_{y}}.$$
 (4.88)

The fully discrete Laplacian operator is defined by

$$\Delta_h = d_x(D_x \phi) + d_y(D_y \phi). \tag{4.89}$$

In particular,

$$\langle f, g \rangle = h_x h_y \sum_{i=1}^{N_x} \sum_{j=1}^{N_y} f_{i,j} g_{i,j},$$
  
 $\|f\|_d = \sqrt{\langle f, f \rangle}.$  (4.90)

Replacing the differential operators in the semidiscrete schemes by the discrete operators properly, we obtain the fully discrete schemes. The energy stability and volume-preserving property are retained in the fully discrete schemes as well (See Appendix-B). For more details on the spatial discretization, we refer readers to the papers [6,8].



#### 4.2.1 The Solvability of the Full-Discrete Scheme

From the Sherman-Morrison formula (See Appendix-A), we notice that the solution uniqueness of

$$A\phi^{n+1} + \sum_{i=1}^{N} \langle \phi^{n+1}, c_i \rangle d_i = b^n$$
 (4.91)

depends on the uniqueness of the corresponding linear system  $A\phi^{n+1} = b^n$  after the spatial discretization at sufficiently small  $\delta t$ . Now we only need to prove the uniqueness of the solution for

$$A\phi^{n+1} = b^n \tag{4.92}$$

for small  $\delta t$ , where  $A = \mathbf{I} + \delta t \overline{M}^{n+1/2} (-\frac{\gamma_1}{2} \Delta_h + \gamma_2 \mathbf{I} + (\overline{q'}^{n+1/2})^2)$ . Since A is symmetric and positive definite, the uniqueness of the solution is apparent.

#### 5 Numerical Results and Discussions

In this section, we conduct mesh refinement tests to validate the accuracy of the proposed schemes and then present some numerical examples to assess the schemes for the nonlocal Allen-Cahn models against those for the Allen-Cahn model and the Cahn–Hilliard model. When considering the definition of the volume in the Allen-Cahn model with a Lagrange multiplier, we use two different choices of  $h(\phi)$ . If  $h(\phi) = \phi$ , we call it model 1, otherwise we name it model 2. For convenience, we refer the numerical schemes designed by EQ strategy for the Allen-Cahn model, the Allen-Cahn model with the penalizing potential, Lagrangian model 1 and 2, and the Cahn–Hilliard model as AC-EQ, AC-P-EQ, AC-L1-EQ, AC-L2-EQ, CH-EQ, respectively. Similarly, we name the numerical schemes obtained using SAV approaches for the models as AC-SAV, AC-P-SAV, AC-L1-SAV, AC-L2-SAV, CH-SAV, respectively.

In the following, we set  $\eta = 1 \times 10^5$  in the EQ and SAV schemes for the Allen-Cahn model with a penalizing potential unless noted otherwise. In addition, we set the constant in the free energy at  $C_0 = 1 \times 10^5$  in all computations.

#### 5.1 Mesh Refinement

We refine the mesh systematically to test the accuracy by setting  $\gamma_1 = \gamma \epsilon = 1 \times 10^{-1}$  and  $\gamma_2 = \frac{\gamma}{\epsilon} = 10$  with the double well potential given in (2.1)and the initial condition given by

$$\phi(0, x, y) = \frac{1}{2} + \frac{1}{2}\cos(\pi x)\cos(\pi y). \tag{5.1}$$

The computational domain is set as  $\Omega = [-1, 1]^2$ . We choose the solution obtained at  $\delta t = 10^{-4}$  and  $\Delta x = \Delta y = \frac{1}{256}$  as the "exact solution". In Tables 1 and 2, we list the  $L^2$  errors of the phase variable between the numerical solutions and the "exact solution" at t = 2 with respect to different time steps. In Tables 1 and 2, we show the convergence rates match second order accuracy with respect to different time steps,  $\delta t = 5 \times 10^{-4}$ ,  $10^{-3}$ ,  $5 \times 10^{-3}$ ,  $10^{-2}$ ,  $5 \times 10^{-2}$ , respectively. We note that the schemes are also second order accurate in space and omit the



Table 1 Numerical errors and convergence rates of the EQ schemes in time

| Scheme   | AC-EQ       |       | AC-P-EQ     |       | AC-L1-EQ    |       | AC-L2-EQ    |       | СН-ЕО       |       |
|----------|-------------|-------|-------------|-------|-------------|-------|-------------|-------|-------------|-------|
| 8t       | $L^2$ Error | Order |
| 5.00E-02 | 2.16E-03    | ı     | 7.68E-07    | I     | 7.80E-07    | ı     | 4.89E-07    | ı     | 1.22E-06    | ı     |
| 1.00E-02 | 3.63E-04    | 1.11  | 7.14E-08    | 1.48  | 7.17E-08    | 1.48  | 4.46E-08    | 1.49  | 4.88E-08    | 2.00  |
| 5.00E-03 | 9.71E-05    | 1.90  | 2.05E-08    | 1.80  | 2.05E-08    | 1.81  | 1.29E-08    | 1.79  | 1.22E-08    | 2.00  |
| 1.00E-03 | 3.93E-06    | 1.99  | 9.14E-10    | 1.93  | 8.86E-10    | 1.95  | 5.78E-10    | 1.93  | 4.83E-10    | 2.01  |
| 5.00E-04 | 9.52E-07    | 2.05  | 2.25E-10    | 2.02  | 1.99E-10    | 2.15  | 1.37E-10    | 2.08  | 1.18E-10    | 2.03  |
|          |             |       |             |       |             |       |             |       |             |       |



Table 2 Numerical errors and convergence rates of the SAV schemes in time

|          |             | )     |             |       |             |       |             |       |             |       |
|----------|-------------|-------|-------------|-------|-------------|-------|-------------|-------|-------------|-------|
| Scheme   | AC-SAV      |       | AC-P-SAV    |       | AC-L1-SAV   |       | AC-L2-SAV   |       | CH-SAV      |       |
| 81       | $L^2$ Error | Order |
| 5.00E-02 | 9.77E-04    | ı     | 1.41E-07    | ı     | 1.40E-07    | ı     | 2.86E-07    | ı     | 1.22E-06    | ı     |
| 1.00E-02 | 1.26E-04    | 1.27  | 9.80E-09    | 1.66  | 9.73E-09    | 1.66  | 1.83E-08    | 1.71  | 4.18E-08    | 2.00  |
| 5.00E-03 | 3.08E-05    | 2.03  | 2.72E-09    | 1.85  | 2.70E-09    | 1.85  | 5.02E-09    | 1.87  | 1.22E-08    | 2.00  |
| 1.00E-03 | 1.12E-06    | 2.06  | 1.18E-10    | 1.95  | 1.17E-10    | 1.95  | 2.14E-10    | 1.96  | 4.83E-10    | 2.01  |
| 5.00E-04 | 2.66E-07    | 2.07  | 2.90E-11    | 2.02  | 2.89E-11    | 2.02  | 5.10E-11    | 2.07  | 1.17E-10    | 2.05  |
|          |             |       |             |       |             |       |             |       |             |       |



| •                | -         |             | *            |              |           |
|------------------|-----------|-------------|--------------|--------------|-----------|
| Scheme           | AC-EQ/SAV | AC-P-EQ/SAV | AC-L1-EQ/SAV | AC-L2-EQ/SAV | CH-EQ/SAV |
| Time for EQ (s)  | 27        | 42          | 57           | 58           | 37        |
| Time for SAV (s) | 38        | 41          | 58           | 50           | 53        |

**Table 3** Computational efficiency of the models in 1000 time steps with  $M = 1 \times 10^{-4}$ 

**Table 4** Computational efficiency of the models in 1000 time steps with  $M = 1 \times 10^{-2}$ 

| Scheme           | AC-EQ/SAV | AC-P-EQ/SAV | AC-L1-EQ/SAV | AC-L2-EQ/SAV | CH-EQ/SAV |
|------------------|-----------|-------------|--------------|--------------|-----------|
| Time for EQ (s)  | 27        | 41          | 60           | 60           | 48        |
| Time for SAV (s) | 37        | 41          | 57           | 53           | 60        |

details of the mesh refinement tests in space. If readers are interested in the error estimate for the Allen-Cahn equation with nonlocal constraints, please refer to [51].

We also test the performance of the schemes when implemented with respect to the initial condition in terms of the computational efficiency. In Table 3, we list the performance of the ten schemes computed in 1000 time steps. The performance depends on the mobility, the other model parameters as well as the initial condition. In the tests conducted with the chosen parameter values, we observe that the best performance, among the volume preserving schemes, is given by the scheme for the Allen-Cahn model with a penalizing potential at  $M = 1 \times 10^{-4}$  for the initial condition given in Eq. (5.1). The performance of the schemes computed using  $M = 1 \times 10^{-2}$  is given in Table 4. The scheme for the Allen-Cahn equation with a penalizing potential once again performs better. The pre-factor of the penalizing term for the Allen-Cahn model with penalizing potential is set at  $\eta = 1 \times 10^5$  in the computations.

In several tests, the performance of EQ is better than that of SAV. This is because that the SAV scheme needs to solve one more linear equation than that of the EQ scheme does. In the case where mobility is larger, the performance of the SAV schemes improves and some even surpasses that of the corresponding EQ schemes. Overall, the performance of the schemes between the EQ and the SAV schemes is comparable.

#### 5.2 Assessment of the Numerical Schemes

In this section, we will assess the numerical schemes derived by using EQ and SAV methods on two benchmark problems. Firstly, we study merging of two drops using the numerical schemes to examine the volume preserving property of the nonlocal models as well as energy dissipation, where the double well potential (2.1) is adopted.

We put two drops, next to each other, in the computational domain. The drops and the ambient are represented by  $\phi=1$  and  $\phi=0$ , respectively. The parameter values of the models are chosen as  $\gamma_1=1\times 10^{-2}$ ,  $\gamma_2=100$ . The initial condition is given by

$$\begin{cases}
1, & r_1 \le 0.2 - \delta \text{ or } r_2 \le 0.2 - \delta, \\
\tanh(\frac{0.2 - r_1}{\delta}), & 0.2 - \delta < r_1 \le 0.2, \\
\tanh(\frac{0.2 - r_2}{\delta}), & 0.2 - \delta < r_2 \le 0.2, \\
0, & \text{other,} 
\end{cases}$$
(5.2)

where 
$$r_1 = \sqrt{(x - 0.3)^2 + (y - 0.5)^2}$$
,  $r_2 = \sqrt{(x - 0.7)^2 + (y - 0.5)^2}$  and  $\delta = 0.01$ .



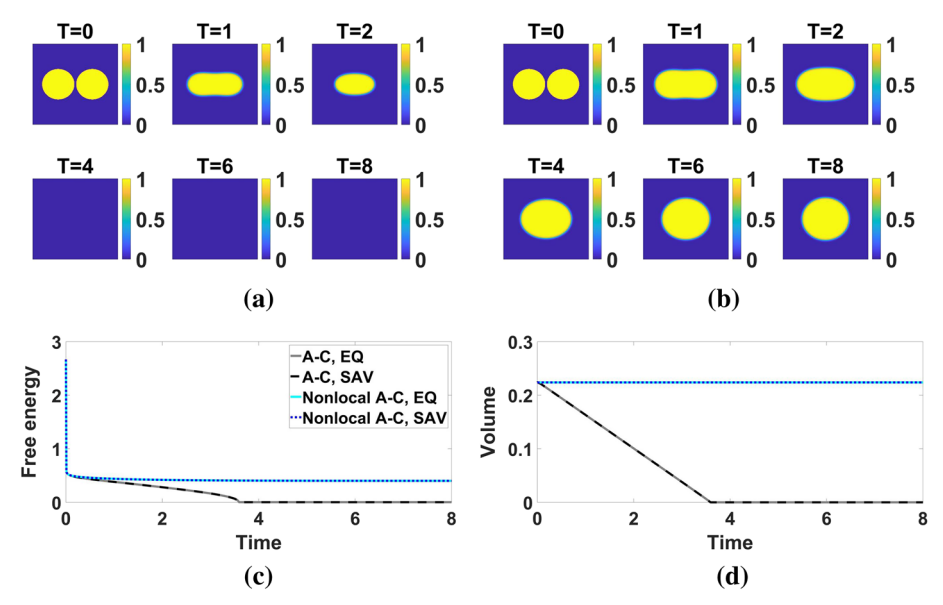


Fig. 1 Merging of two drops simulated using the Allen-Cahn and the Allen-Cahn models with nonlocal constraints at M=1. The drop dynamics of the Allen-Cahn model and the Allen-Cahn model with nonlocal constraints are shown in  $\bf a$  and  $\bf b$  computed using the AC-EQ and AC-L1-SAV scheme, respectively. Snapshots of the numerical approximation of  $\bf \varphi$  are taken at T=0,0.8,1.6,2.4,3.2,4, respectively, in both cases. The time evolution of the free energy and phase volume are shown in  $\bf c$  and  $\bf d$ , respectively. Since all other models except for the Allen-Cahn model predict similar dynamical behavior, we only show the phase transition dynamics computed using the AC-L1-SAV scheme in  $\bf b$ . We compare the time evolution of the free energy and volume computed by the EQ and SAV schemes in  $\bf c$  and  $\bf d$ . The volume computed using the Allen model vanishes before  $\bf T=4$  and in the meantime the energy hits zero as well. All nonlocal Allen-Cahn models preserve the volume and dissipate energies in time.  $\bf Y_1=1\times10^{-2},\,\bf Y_2=100$  are used in the computations and the temporal and spatial step sizes are set as  $\bf \delta t=1\times10^{-5}$  and  $\bf h_x=h_y=1/256$ , respectively

We first simulate merging of two drops using the Allen-Cahn model as well as the Allen-Cahn model with nonlocal constraints, respectively, where M=1. The results computed from the EQ and SAV schemes for the Allen-Cahn model are identical, likewise the results computed using the EQ and SAV schemes for the nonlocal Allen-Cahn models are identical. We don't see any differences between the results of the Allen-Cahn model with a penalizing potential and those of the Allen-Cahn model of a Lagrange multiplier. Figure 1a depicts the results computed from AC-EQ scheme and Fig. 1b shows the results computed from AC-L1-SAV. We show these two simulations as representative examples.

From the simulations, we observe that drops computed using the Allen-Cahn model first merge into a single drop and then the drop dissipates until eventually vanishes at the end of the simulation; while drops computed using the Allen-Cahn models with nonlocal constraints merge into a single drop and eventually rounded up at the end of the simulation. Figure 1c and d depict the computed free energy and volume of drops using the two numerical schemes. Obviously, the volume decays in the Allen-Cahn model while is conserved in the simulation of the other models. The free energy decays in the Allen-Cahn model with respect to time and vanishes as the drop disappears. In contrast, the free energy of the Allen-Cahn model with a nonlocal constraint saturates at a nonzero value at the end of the simulation.



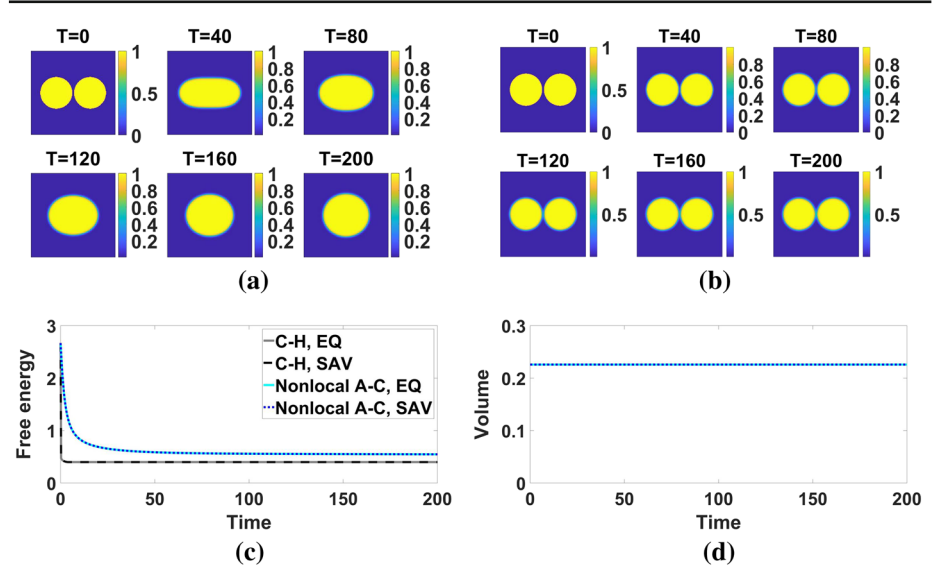


Fig. 2 Merging of two drops simulated using the Cahn–Hilliard and the Allen-Cahn models with nonlocal constraints at  $M=1\times 10^{-4}$ . The phase evolution of the drops using the CH-EQ and AC-L1-SAV scheme is shown in **a** and **b**, respectively. Snapshots of the numerical solution of  $\phi$  are taken at T=0, 40, 80, 120, 160, 200, respectively, in both simulations. The time evolution of the free energy and the volume are shown in **c** and **d**, respectively. The Cahn–Hilliard model and the nonlocal Allen-Cahn models preserve the volume of each phase and dissipate energies in time. Since the energy dissipates faster in the Cahn–Hilliard model than in the nonlocal Allen-Cahn models initially, the energy profile predicted by the former is lower than the one predicted by the latter in the simulations. We set  $\gamma_1=1\times 10^{-2}$ ,  $\gamma_2=100$  in the simulations. The temporal and spatial steps are set as  $\delta t=1\times 10^{-5}$  and  $h_x=h_y=1/256$ , respectively

Then, we repeat the simulations using the Allen-Cahn model with nonlocal constraints and the Cahn–Hilliard model with mobility  $M=1\times 10^{-4}$ . Since the coarsening rate in the Cahn–Hilliard model is much faster than that in the nonlocal Allen-Cahn models. At T=200, the drops described by the Cahn–Hilliard model have merged into a single rounded drop, while the drops described by the nonlocal Allen-Cahn model just begin fusing. Figure 2a and b depict a representative drop merging simulation using the CH-EQ scheme for the Cahn–Hilliard model and one using the AC-L1-SAV scheme for the Allen-Cahn model with a Lagrange multiplier, respectively. The time evolution of the free energy computed from the Cahn–Hilliard model and that from the nonlocal Allen-Cahn model is depicted in Fig. 2c and d, respectively, in which the Cahn–Hilliard model yields a smaller free energy than the nonlocal Allen-Model. This is because at T=200 the Cahn–Hilliard dynamics has come into a steady state comparing with the dynamics of the Allen-Cahn model with nonlocal constraints.

Secondly we use a random initial condition to assess the property of volume preserving nonlocal Allen-Cahn models in phase coarsening dynamics. Once again, The Allen-Cahn model gives one phase diagram at t=50, while the Allen-Cahn models with nonlocal constraints yield another at the same parameter values and initial conditions. There is simply no comparison between these two model predictions in the terminal phase diagram. Figure 3a and b depict typical simulations using the AC-EQ scheme for the Allen-Cahn model and the AC-L1-EQ scheme for the Allen-Cahn model with a Lagrangian multiplier, respectively. The time evolution of the free energy and the volume computed from the numerical schemes for



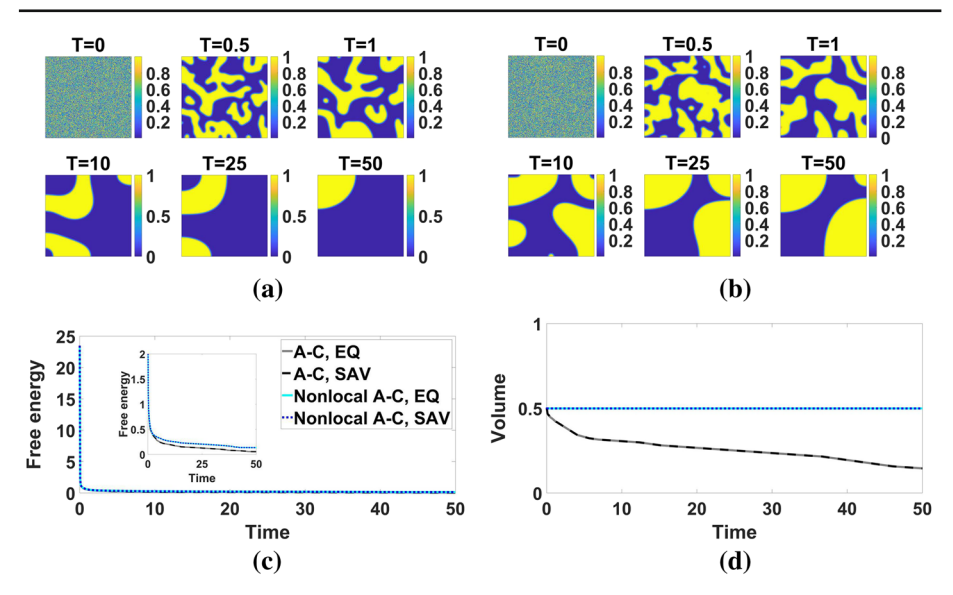


Fig. 3 Coarsening dynamics simulated using the Allen-Cahn and the Allen-Cahn models with nonlocal constraints at M=1. The coarsening dynamics computed using the AC-EQ and AC-L1-EQ scheme are shown in  $\bf a$  and  $\bf b$ , respectively. Snapshots of the numerical solution of  $\bf \phi$  are taken at T=0,0.5,1,10,25,50, respectively, in both cases. The time evolution of the free energy and the volume are shown in  $\bf c$  and  $\bf d$ , respectively. The Allen-Cahn model does not conserve the volume, while the nonlocal Allen-Cahn models preserve the volume of each phase and dissipate energies in time. The energy obtained using the Allen-Cahn model is lower than that using the nonlocal Allen-Cahn models. We set  $\gamma_1=2\times 10^{-3}, \gamma_2=50$  in the computations. The temporal and spatial step sizes are set at  $\delta t=1\times 10^{-5}$  and  $h_x=h_y=1/256$ , respectively

the models are shown in Fig. 3c and d, respectively. Between the EQ and SAV schemes of the same model, we have yet seen any visible differences from the numerical results.

The behavior of such coarsening dynamics is also compared between the Cahn-Hilliard model and the nonlocal Allen-Cahn models. Since the coarsening rate in the Cahn-Hilliard model is faster than that in the nonlocal Allen-Cahn models, we increase the magnitude of the mobility coefficient in the Allen-Cahn model with nonlocal constraints by 1000 folds and then repeat the simulations. This speeds up the coarsening dynamics of the nonlocal Allen-Cahn system significantly, although the result from the Cahn-Hilliard model still reaches a coarser grain than that of the Allen-Cahn models with nonlocal constraints. Figure 4a and b depict two representative examples on phase coarsening dynamics using CH-SAV and AC-L1-SAV schemes, respectively. Figure 4c and d show the decaying free energy and the volume preserving results for the two selected simulations.

The results show the classical, non-volume-conserving Allen-Cahn model can't be used to simulate the merging of drops and the coarsening dynamics accurately, whereas the nonlocal Allen-Cahn models and the Cahn-Hilliard model can (see Figs. 1–4). Compared with the Allen-Cahn model and the Cahn-Hilliard model, the nonlocal Allen-Cahn models not only conserves the volume of each phase, but also shows a slower dissipation rate. One can enlarge the mobility of the nonlocal Allen-Cahn models to accelerate dynamics of merging. We also compared the time evolution of the dissipation rates for the nonlocal Allen-Cahn models and the Cahn-Hilliard model with the same mobility coefficient M. The result indicates that the dissipation rate of the nonlocal Allen-Cahn models is slower than that of the Cahn-Hilliard model (see Fig. 5).



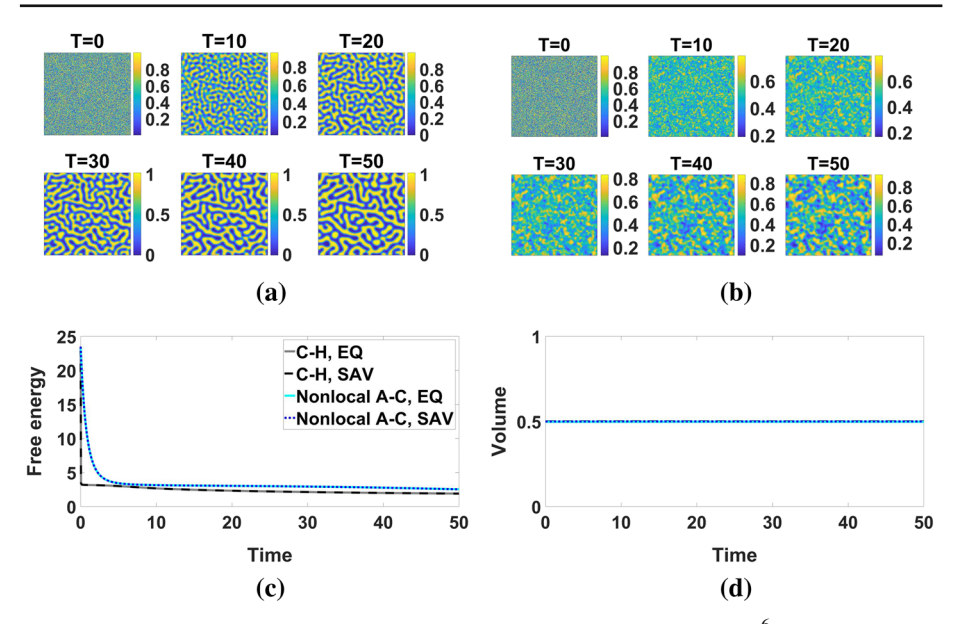
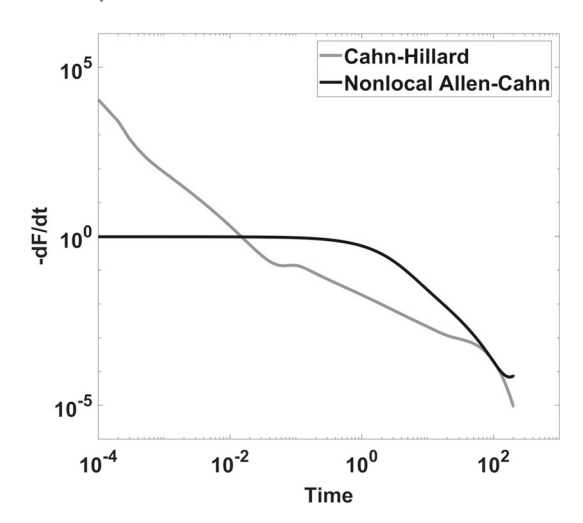
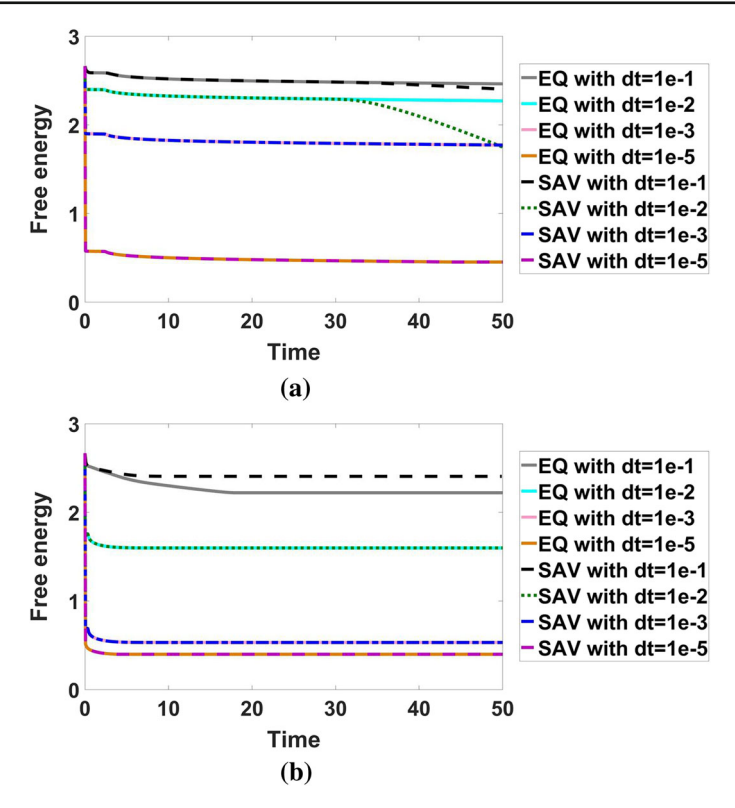


Fig. 4 Coarsening dynamics simulated using the Cahn–Hilliard model at  $M=1\times 10^{-6}$  and the Allen-Cahn models with nonlocal constraints at  $M=1\times 10^{-3}$ . The coarsening dynamics of the Cahn–Hilliard model and the Allen-Cahn model with nonlocal constraints are shown in **a** and **b**, simulated using corresponding SAV schemes (CH-AV and AC-L1-SAV), respectively. Snapshots of the numerical solution of  $\phi$  are taken at T=0,10,20,30,40,50 in both cases. The time evolution of the free energy and volume are shown in **c** and **d**, respectively. All models preserve the volume of each phase and dissipate energies in time. The faster coarsening dynamics in the Cahn–Hilliard model makes its energy slightly lower than the one predicted using the nonlocal Allen-Cahn models. We set  $\gamma_1=2\times 10^{-3}$ ,  $\gamma_2=50$  in the computations. The temporal and spatial step sizes are set at  $\delta t=1\times 10^{-5}$  and  $h_x=h_y=1/256$ , respectively

Fig. 5 Time evolution of the magnitude of the dissipation rate with the Cahn-Hilliard model and the Allen-Cahn model with nonlocal constraints, simulated using CH-EQ and AC-L1-SAV, respectively. The dissipation rate of the energy is calculated from Fig. 2. At t < 0.02, the dissipation rate in the Cahn-Hilliard equation is larger than that in the Allen-Cahn equations with nonlocal constraints. The strong energy decay initially is a result of enhanced mixing. This explains why the Cahn-Hilliard dynamics merges drops faster than that of the Allen-Cahn model with nonlocal constraints







**Fig. 6** Comparison on accuracy of numerical solutions of the Cahn–Hilliard model and the Allen-Cahn model with a Lagrange multiplier. **a** The free energy computed using the Cahn–Hilliard model at four selected time steps, respectively. **b**. The free energy computed using AC-L1-EQ and AC-L1-SAV schemes at four selected time steps, respectively. The time step sizes used are  $1 \times 10^{-1}$ ,  $1 \times 10^{-2}$ ,  $1 \times 10^{-3}$ ,  $1 \times 10^{-5}$ . We use  $M = 1 \times 10^{-4}$  for the Cahn–Hilliard model and M = 1 for the nonlocal Allen-Cahn model. The initial condition and other model parameters are the same as those in Fig. 2. In the computation using the Cahn–Hilliard model, the result converges at  $\delta t = 1 \times 10^{-5}$ . The outcome is slightly better for the Allen-Cahn model with a lagrange multiplier

#### 5.2.1 Practical Implementation of the Schemes

Although the schemes are shown unconditionally energy stable, the numerical results are not guaranteed to be always accurate if the time step size is large due to the sequential decoupling of the schemes in Fig. 6. In all these schemes based on the energy quadratization strategy, the equations for the auxiliary variables or the intermediate variables are ordinary differential equations, derived from the original algebraic equations (which define the intermediate variables) by taking time derivatives. Although the reformulated equation system is equivalent to the original one, the numerical schemes devised to solve these differential equations may not be accurate enough to warrant the solution is obtained accurately at large time steps. This is an accuracy issue in the numerical simulation.

To remedy the inherent deficiency, we propose two methods to modify the schemes in practical implementations to improve their numerical accuracy with a large time step. For simplicity, we define  $f_1(\phi^n)$  as the non-quadratic, nonlinear term in the bulk potential, which is  $f_1(\phi^n) = f(\phi^n) - \gamma_2(\phi^n)^2$  in this paper. The two methods are given below.



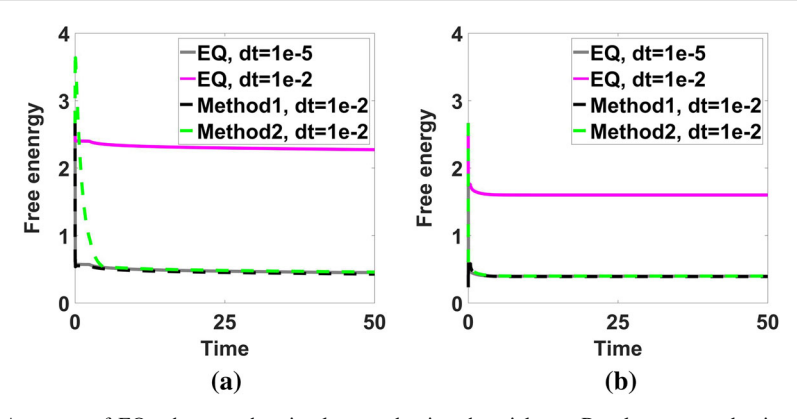


**Fig. 7** Accuracy of EQ schemes when implemented using the tricks. **a.** Results computed using CH-EQ scheme. **b.** Results computed using the AC-L1-EQ scheme. We use  $M = 1 \times 10^{-4}$ ,  $\alpha = 1$ ,  $C = 5 \times 10^{-5}$  for the Cahn–Hilliard model and M = 1,  $\alpha = 1$ ,  $C = 1.5 \times 10^{-4}$  for the Allen-Cahn model with a Lagrange multiplier in the simulations. The second numerical trick works better than the first one in the case of the nonlocal Allen-Cahn model, but the first method works better for the Cahn–Hilliard model. The initial conditions and the parameter values are the same as those used in Fig. 2

- 1. After obtaining  $\phi^{n+1}$ , we update  $q^{n+1}$  using  $q^{n+1} = \sqrt{f_1(\phi^{n+1}) + C_0}$  instead of solving the ordinary equation of q.
- 2. After obtaining  $\phi^{n+1}$ , if  $\int_{\Omega} (q^{n+1} \sqrt{f_1(\phi^{n+1}) + C_0}) d\mathbf{x} \leqslant \varepsilon$  for a prescribed  $\varepsilon > 0$ , we update  $q^{n+1}$  using  $q^{n+1} = q^n + \overline{q'}^{n+1/2}(\phi^{n+1} \phi^n)$ , otherwise, using  $q^{n+1} = \sqrt{f_1(\phi^{n+1}) + C_0} \frac{2-\alpha\delta t}{2+\alpha\delta t}(q^n \sqrt{f_1(\phi^n) + C_0})$ .

In method 1, we update the value of  $q^{n+1}$  using the original definition of q after  $\phi^{n+1}$  is obtained each step. In method 2, we introduce an additional decay mechanism for the quantify  $q - \sqrt{f_1(\phi) + C_0}$  as follows

$$\left(q - \sqrt{f_1(\phi) + C_0}\right)_t = -\alpha (q - \sqrt{f_1(\phi) + C_0}), \alpha > 0.$$
 (5.3)

If  $\alpha=0$ , this equation recovers the reformulated equation for the intermediate variable q. When  $\alpha>0$ , it serves as decay equation to reduce  $\sqrt{f_1(\varphi)+C_0}$  in time. We note that, in method 2, the result is insensitive to the choice of  $\alpha>0$ . Figure 6 depicts a pair of comparative studies on drop merging simulations using the Cahn–Hilliard model and the Allen-Cahn model with a Lagrange multiplier discretized using both EQ and SAV methods. The benchmark results are obtained using small time steps. Using these two tricks, we can alleviate the constraints imposed on the time step size for the EQ schemes considerably. In Fig. 7, we show results of the numerical methods at a relatively large step size. The improvement is significant. We also test the tricks on the SAV schemes, however we observe that only method 1 performs well.

In the numerical experiments, we observe that the Allen-Cahn model with a penalizing potential and the Allen-Cahn model with a Lagrange multiplier seem to render comparable numerical results. In this study, we have used two different definitions of the phase volume  $V(t) = \int_{\Omega} h(\phi(t)) d\mathbf{x}$  with two choices of  $h(\phi)$ :

$$h(\phi) = \phi,$$

$$h'(\phi) = \frac{(m+1)(2m+1)}{m} [\phi(1-\phi)]^m, m \text{ is a positive integer.}$$
(5.4)

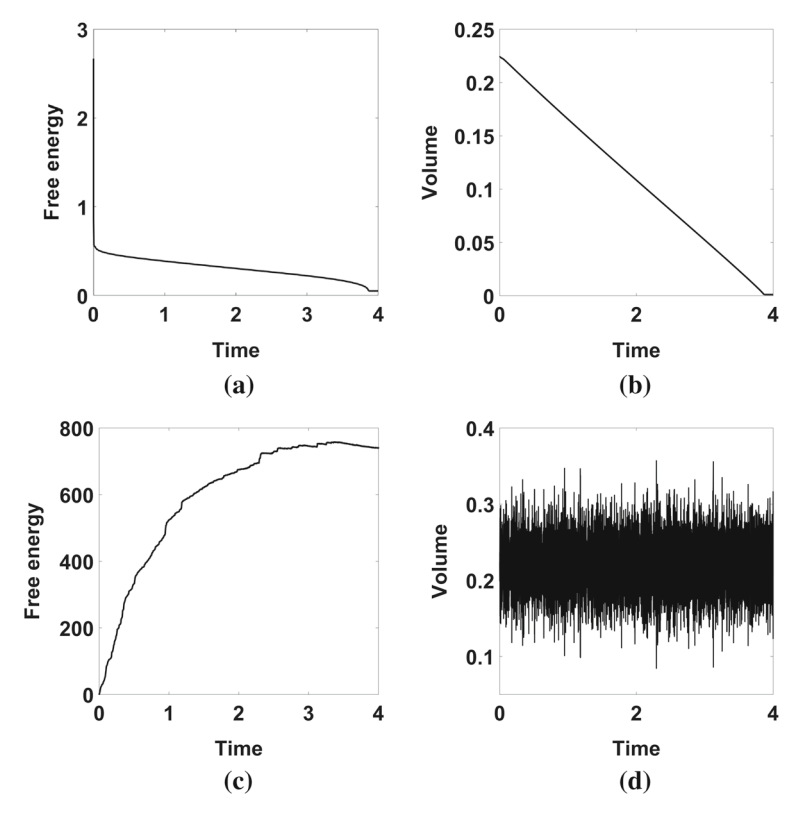


Fig. 8 Two examples of failure for the Allen-Cahn model with a penalizing potential at M=1, where  $\eta=1$  and  $\eta=1\times 10^{18}$  are chosen in the simulations. We plotted time evolution of the free energy and the volume, respectively. Results in **a** and **b** are obtained using the AC-P-EQ scheme with  $\eta=1$ . Results in **c** and **d** are obtained using the AC-P-SAV scheme with  $\eta=1\times 10^{18}$ . The time step size and space time size are chosen as  $\delta t=1\times 10^{-5}$ ,  $h_x=h_y=1/256$  in the simulations, respectively. The initial conditions and other parameters are chosen the same as those in Fig. 2. These show that if  $\eta$  is not "properly chosen", the results are not volume-conserving nor energy stable

Our numerical experiments do not seem to be able to differentiate between the nonlocal Allen-Cahn models using either definitions. Thus, both can be used at the discretion of the user in practice. Physically, the second definition seems to be more sound because the compensation to the time change of the volume fraction primarily takes place around the interface while the first definition seems to compensate the phase variable globally [18].

The phase evolution, time evolution of the volume and the free energy of the two Allen-Cahn models with nonlocal constraints simulated by EQ or SAV are essentially the same, if the penalizing parameter  $\eta$  is chosen appropriately. The choice of  $\eta$  can be fairly arbitrary [17]. For very large  $\eta$ , however, the code does not perform well in that it slows down significantly due to stiffness of the system. We thus believe there exists an "optimal"  $\eta$  that renders the best result, which ought to be determined empirically in numerical implementations. We show two examples of failure at either large  $\eta$  or a small  $\eta$  in Fig. 8, in which the energy is not dissipative nor the volume conserved.

In the case with a double well potential, if we define  $q^2 = \gamma_2 \phi^2 (1 - \phi)^2$  rather than the one in Sect. 4.1 in the schemes, we observe a significant improvement in convergence



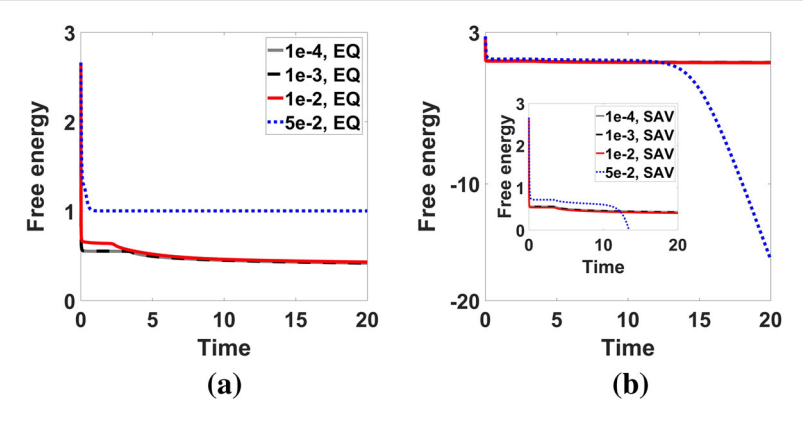


Fig. 9 Merging of two drops simulated by the AC-L1-EQ scheme in **a** and the AC-L1-SAV scheme in **b**. The time step sizes used are  $1\times10^{-4}$ ,  $1\times10^{-3}$ ,  $1\times10^{-2}$ ,  $5\times10^{-2}$ , respectively. The spatial mesh is  $256\times256$  in 2D. The initial conditions and other parameter values are the same as those in Fig. 2. At a relatively large step size  $\delta t = 0.05$ , the scheme AC-L1-SAV yields an erroneous result

at large time steps. The same results are also observed in [43]. This is because  $q' = \frac{\delta q}{\delta \varphi} = \sqrt{\gamma_2}(1-2\varphi)$  is a linear function, the extrapolation  $\overline{q'}^{n+1/2} = \frac{3}{2}(q')^n - \frac{1}{2}(q')^{n-1}$  or  $\overline{q'}^{n+1/2} = q'(\frac{3}{2}\varphi^n - \frac{1}{2}\varphi^{n-1})$  is exact! Compared with the results computed by previous schemes with large time steps for nonlocal models in Fig. 6, larger time steps can perform well in the newly developed EQ or SAV schemes in Fig. 9. Notice that EQ schemes outperform SAV schemes at  $\delta t = 5 \times 10^{-2}$  but under-perform SAV schemes at  $\delta t = 1 \times 10^{-2}$ , where the SAV scheme fails after some time. Their performance is therefore comparable on average.

#### 6 Conclusions

We have developed an exhaustive set of linear, second order, energy stable schemes for the Allen-Cahn equation with nonlocal constraints that preserve the phase volume and compared them with the energy stable, linear schemes for the Allen-Cahn and the Cahn—Hilliard models. These schemes are devised based on the energy quadratization strategy in the form of EQ and SAV format. We show that they are unconditionally energy stable and linear systems resulted from them are uniquely solvable. All schemes can be solved using efficient numerical methods, making the models bona fide alternatives to the Cahn—Hilliard model to describe interfacial dynamics of immiscible materials while preserving the volume. The nonlocal Allen-Cahn models exhibit a slower coarsening rate than the Cahn—Hilliard model at the same mobility, but one can increase the mobility coefficient of the nonlocal Allen-Cahn model to accelerate their dynamics.

Two practical implementation tricks are introduced to enhance the accuracy of the numerical schemes at a large step size, but the second method seems to be not working well on the SAV schemes. In addition, we have compared the two Allen-Cahn models with nonlocal constraints numerically. The computational efficiency of the Allen-Cahn model with a penalizing potential is slightly better than the one with a Lagrange multiplier, but the accuracy of the former depends on a suitable choice of model parameter η. Through numerical experiments, we show that the practical implementation using the defining algebraic functions for the auxiliary variable makes the EQ scheme superior to the SAV scheme in the computational



efficiency and accuracy. When the equation of the auxiliary variable can be solved more accurately, large time step size can be applied. In the end, we note that the size of mobility and the time step size are dominating factors that determine ultimately the efficiency and accuracy of the schemes.

**Acknowledgements** This research is partially supported by NSFC Awards #11571032, #91630207 and NSAF-U1530401.

# **Appendix**

# A Sherman-Morrison Formula and its Application to Solving the Integro-Differential Equation

Here we give a brief review on the Sherman-Morrison formula [52] and explain its applications in the practical implementation of our various relevant schemes.

Suppose A is an invertible square matrix, and u,v are column vectors. Then  $A + uv^T$  is invertible iff  $1 + v^T A^{-1}u \neq 0$ . If  $A + uv^T$  is invertible, then its inverse is given by

$$(A + uv^{T})^{-1} = A^{-1} - \frac{A^{-1}uv^{T}A^{-1}}{1 + v^{T}A^{-1}u}.$$
 (A.1)

So if Ay = b and Az = u,  $(A + uv^T)x = b$  has the solution given by

$$x = y - \frac{v^T y}{1 + v^T z} z. \tag{A.2}$$

For the integral term(s) in the semi-discrete schemes in this study such as (4.26), we need to discretize it properly.  $\forall f$ , we discretize  $\int_{\Omega} f d\mathbf{x}$  using the composite trapezoidal rule and adding all the elements of the new matrix  $w_1 w_2^T f$ , where  $w_1 = \frac{h_x}{2} S$ ,  $w_2 = \frac{h_y}{2} S$ ,  $h_x$ ,  $h_y$  are the spatial step sizes and  $S = [1, 2, 2, ..., 2, 2, 1]^T$ . For convenience, we use  $w_1 w_2^T f$  to represent the integral discretized by the composite trapezoidal rule.

To solve Eq. (4.26), we discretize the integral or the inner product of functions  $(c, \phi^{n+1})d$  as  $uv^T\phi^{n+1}$ . The scheme is recast to  $A\phi^{n+1} + uv^T\phi^{n+1} = b^n$ . After using the Sherman-Morrison formula, we get

$$\phi^{n+1} = A^{-1}b^n - \frac{v^T A^{-1}b^n}{1 + v^T A^{-1}u}A^{-1}u, \tag{A.3}$$

In the inner product of vectors, (4.26) can be rewritten into

$$\phi^{n+1} = A^{-1}b^n - \frac{\langle c, A^{-1}b^n \rangle}{1 + \langle c, A^{-1}d \rangle} A^{-1}d. \tag{A.4}$$

So, indeed the approach we take in the study using discrete inner product is essentially equivalent to applying the Sherman-Morrison formula.

# B The Energy Dissipation Theorem in the Full Discrete Scheme

Here we only give the energy dissipation theorem in the full discrete scheme for the Allen-Cahn model with a penalizing potential, since the others are similar.



**Theorem B.1** The full discrete scheme in (4.23) obeys the following energy dissipation law

$$F^{n+1} - F^n = -\delta t \langle \tilde{\mu}^{n+1/2}, \overline{M}^{n+1/2} \tilde{\mu}^{n+1/2} \rangle.$$
 (B.1)

Hence, it is unconditionally stable.

**Proof** Taking the  $l^2$  inner product of  $\frac{\Phi^{n+1}-\Phi^n}{\delta t}$  with  $-\tilde{\mu}^{n+1/2}$ , we obtain

$$-\left\langle \frac{\Phi^{n+1} - \Phi^{n}}{\delta t}, \tilde{\mu}^{n+1/2} \right\rangle = \langle \overline{M}^{n+1/2} [\mu^{n+1/2} + \sqrt{\eta} \zeta^{n+1/2}], \mu^{n+1/2} + \sqrt{\eta} \zeta^{n+1/2} \rangle$$

$$= \left\| \sqrt{\overline{M}^{n+1/2}} \left( \mu^{n+1/2} + \sqrt{\eta} \zeta^{n+1/2} \right) \right\|_{d}^{2}, \tag{B.2}$$

Taking the  $l^2$  inner product of  $\tilde{\mu}^{n+1/2}$  with  $\frac{\Phi^{n+1}-\Phi^n}{\delta t}$ , we obtain

$$\left\langle \left( -\gamma_{1} \nabla_{h}^{2} \phi + 2 \gamma_{2} \phi \right)^{n+1/2} + 2 q^{n+1/2} \overline{q'}^{n+1/2} + \sqrt{\eta} \xi^{n+1/2}, \frac{\phi^{n+1} - \phi^{n}}{\delta t} \right\rangle$$

$$= \frac{\gamma_{1}}{2\delta t} (\|\nabla_{h} \phi^{n+1}\|_{d}^{2} - \|\nabla_{h} \phi^{n}\|_{d}^{2}) + \frac{\gamma_{2}}{\delta t} (\|\phi^{n+1}\|_{d}^{2} - \|\phi^{n}\|_{d}^{2})$$

$$+ \left\langle 2 q^{n+1/2} \overline{q'}^{n+1/2}, \frac{\phi^{n+1} - \phi^{n}}{\delta t} \right\rangle + \left\langle \sqrt{\eta} \xi^{n+1/2}, \frac{\phi^{n+1} - \phi^{n}}{\delta t} \right\rangle. \tag{B.3}$$

Taking the  $l^2$  inner product of  $q^{n+1} - q^n$  with  $\frac{q^{n+1} + q^n}{\delta t}$ , we obtain

$$\frac{1}{\delta t}(\|q^{n+1}\|_d^2 - \|q^n\|_d^2) = \frac{1}{\delta t}\langle \overline{q'}^{n+1/2}(\phi^{n+1} - \phi^n), q^{n+1} + q^n\rangle.$$
 (B.4)

Taking the  $l^2$  inner product of  $\zeta^{n+1} - \zeta^n$  with  $\frac{\zeta^{n+1} + \zeta^n}{\delta t}$ , we obtain

$$\frac{1}{8t}(\|\xi^{n+1}\|_d^2 - \|\xi^n\|_d^2) = \frac{1}{8t}\langle\sqrt{\eta}\|\phi^{n+1} - \phi^n\|_d^2, \xi^{n+1} + \xi^n\rangle. \tag{B.5}$$

Combining the above equations, we have

$$\frac{\gamma_{1}}{2\delta t}(\|\nabla_{h}\phi^{n+1}\|_{d}^{2} - \|\nabla_{h}\phi^{n}\|_{d}^{2}) + \frac{\gamma_{2}}{\delta t}(\|\phi^{n+1}\|_{d}^{2} - \|\phi^{n}\|_{d}^{2}) 
+ \frac{1}{\delta t}(\|q^{n+1}\|_{d}^{2} - \|q^{n}\|_{d}^{2}) + \frac{1}{2\delta t}(\|\zeta^{n+1}\|_{d}^{2} - \|\zeta^{n}\|_{d}^{2}) 
= - \left\|\sqrt{\overline{M}^{n+1/2}}(\mu^{n+1/2} + \sqrt{\eta}\zeta^{n+1/2})\right\|_{d}^{2}.$$
(B.6)

This proves the energy stability equality.

#### References

- Allen, S.M., Cahn, J.W.: A microscopic theory for antiphase boundary motion and its application to antiphase domain coarsening. Acta Metallurgica 27(6), 1085–1095 (1979)
- Cahn, J.W., Hilliard, J.E.: Free energy of a nonuniform system. i. interfacial free energy. J. Chem. Phys. 28(2), 258–267 (1958)



- Gurtin, M.E., Polignone, D., Vinals, J.: Two-phase binary fluids and immiscible fluids described by an order parameter. Math. Models Methods Appl. Sci. 6(06), 815–831 (1996)
- Doi, M., Edwards, S.F.: The Theory of Polymer Dynamics, vol. 73. Oxford University Press, Oxford (1988)
- 5. Leslie, F.M.: Theory of flow phenomena in liquid crystals. Adv. Liq. Cryst. 4, 1–81 (1979)
- Gong, Y., Zhao, J., Yang, X., Wang, Q.: Fully discrete second-order linear schemes for hydrodynamic phase field models of binary viscous fluid flows with variable densities. SIAM J. Sci. Comput. 40(1), B138–B167 (2018)
- Pethrick, R.A.: The theory of polymer dynamics m. doi and s. f. edwards, oxford university press. J. Chem. Technol. Biotechnol. 44(1), 79–80 (1988)
- Gong, Y., Zhao, J., Wang, Q.: Linear second order in time energy stable schemes for hydrodynamic models
  of binary mixtures based on a spatially pseudospectral approximation. Adv. Comput. Math. 44(5), 1573

  1600 (2018)
- Yang, X., Lili, J.: Linear and unconditionally energy stable schemes for the binary fluid-surfactant phase field model. Comput. Methods Appl. Mech. Eng. 318, 1005–1029 (2017)
- Zhao, J., Wang, Q., Yang, X.: Numerical approximations to a new phase field model for two phase flows of complex fluids. Comput. Methods Appl. Mech. Eng. 310, 77–97 (2016)
- Zhao, J., Wang, Q., Yang, X.: Numerical approximations for a phase field dendritic crystal growth model based on the invariant energy quadratization approach. Int. J. Numer. Methods Eng. 110(3), 279–300 (2017)
- Wise, S.M., Wang, C., Lowengrub, J.S.: An energy-stable and convergent finite-difference scheme for the phase field crystal equation. SIAM J. Numer. Anal. 47(3), 2269–2288 (2009)
- Yang, X., Gong, Y., Li, J., Zhao, J., Wang, Q.: On hydrodynamic phase field models for binary fluid mixtures. Theor. Comput. Fluid Dynam. 32(5), 1–24 (2017)
- Cheng, Y., Kurganov, A., Zhuolin, Q., Tang, T.: Fast and stable explicit operator splitting methods for phase-field models. J. Comput. Phys. 303, 45–65 (2015)
- Guo, R., Yan, X.: Local discontinuous galerkin method and high order semi-implicit scheme for the phase field crystal equation. SIAM J. Sci. Comput. 38(1), A105–A127 (2016)
- Qiang, D., Liu, C., Wang, X.: A phase field approach in the numerical study of the elastic bending energy for vesicle membranes. J. Comput. Phys. 198(2), 450–468 (2004)
- 17. Li, H., Lili, J., Zhang, C., Peng, Q.: Unconditionally energy stable linear schemes for the diffuse interface model with peng-robinson equation of state. J. Sci. Comput. **75**(2), 993–1015 (2018)
- Rubinstein, J., Sternberg, P.: Nonlocal reaction diffusion equations and nucleation. IMA J. Appl. Math. 48(3), 249–264 (1992)
- Yang, X., Feng, J.J., Liu, C., Shen, J.: Numerical simulations of jet pinching-off and drop formation using an energetic variational phase-field method. J. Comput. Phys. 218(1), 417–428 (2006)
- Mellenthin, J., Karma, A., Plapp, M.: Phase-field crystal study of grain-boundary premelting. Phys. Rev. B 78(18), 184110 (2008)
- Guillén-González, F., Tierra, G.: On linear schemes for a cahn-hilliard diffuse interface model. J. Comput. Phys. 234, 140–171 (2013)
- Li, D., Qiao, Z.: On second order semi-implicit fourier spectral methods for 2d cahn-hilliard equations.
   J. Sci. Comput. 70(1), 301–341 (2017)
- Elliott, C.M., Stuart, A.M.: The global dynamics of discrete semilinear parabolic equations. SIAM J. Numer. Anal. 30(6), 1622–1663 (1993)
- Fan, X., Kou, J., Qiao, Z., Sun, S.: A componentwise convex splitting scheme for diffuse interface models with van der waals and peng-robinson equations of state. SIAM J. Sci. Comput. 39(1), B1–B28 (2017)
- Eyre, D.J.: Unconditionally gradient stable time marching the cahn-hilliard equation. MRS online proceedings library archive, 529 (1998)
- Shen, J., Wang, C., Wang, X., Wise, S.M.: Second-order convex splitting schemes for gradient flows with ehrlich-schwoebel type energy: application to thin film epitaxy. SIAM J. Numer. Anal. 50(1), 105–125 (2012)
- 27. Wang, C., Wang, X., Wise, S.M.: Unconditionally stable schemes for equations of thin film epitaxy. Discrete Contin. Dyn. Syst. **28**(1), 405–423 (2010)
- Han, D., Wang, X.: A second order in time, uniquely solvable, unconditionally stable numerical scheme for cahn-hilliard-navier-stokes equation. J. Comput. Phys. 290, 139–156 (2015)
- Chuanju, X., Tang, T.: Stability analysis of large time-stepping methods for epitaxial growth models. SIAM J. Numer. Anal. 44(4), 1759–1779 (2006)
- Shen, J., Yang, X.: Numerical approximations of allen-cahn and cahn-hilliard equations. Discrete Contin. Dyn. Syst. 28(4), 1669–1691 (2010)



- Chen, W., Han, D., Wang, X.: Uniquely solvable and energy stable decoupled numerical schemes for the cahn-hilliard-stokes-darcy system for two-phase flows in karstic geometry. Numer. Math. 137(1), 229–255 (2017)
- Wang, L., Yu, H.: On efficient second order stabilized semi-implicit schemes for the cahn-hilliard phasefield equation. J. Sci. Comput. 77(2), 1–25 (2017)
- Qiang, D., Lili, J., Li, X., Qiao, Z.: Stabilized linear semi-implicit schemes for the nonlocal cahn-hilliard equation. J. Comput. Phys. 363, 39–54 (2018)
- Wang, L., Yu, H.: Energy stable second order linear schemes for the allen-cahn phase-field equation. arXiv preprint arXiv:1807.03171 (2018)
- Zhao, J., Yang, X., Gong, Y., Zhao, X., Yang, X., Li, J., Wang, Q.: A general strategy for numerical approximations of non-equilibrium models-part i: thermodynamical systems. Int. J. Numer. Anal. Model. 15(6), 884–918 (2018)
- Yang, X., Zhao, J., Wang, Q.: Numerical approximations for the molecular beam epitaxial growth model based on the invariant energy quadratization method. J. Comput. Phys. 333, 104–127 (2017)
- Shen, J., Jie, X., Yang, J.: The scalar auxiliary variable (sav) approach for gradient flows. J. Comput. Phys. 353, 407–416 (2018)
- 38. Shen, J., Xu, J., Yang, J.: A new class of efficient and robust energy stable schemes for gradient flows. arXiv preprint arXiv:1710.01331, (2017)
- Li, X., Shen, J., Rui, H.: Energy stability and convergence of sav block-centered finite difference method for gradient flows. arXiv preprint arXiv:1812.01793 (2018)
- Dong, S., Yang, Z., Lin, L.: A family of second-order energy-stable schemes for cahn-hilliard type equations. arXiv preprint arXiv:1803.06047 (2018)
- Zhao, J., Gong, Y., Wang, Q.: Aritrary high order unconditionally energy stable schemes for gradient flow models. Submitted to J. Comput. Phys. (2019)
- Chen, L., Zhao, J., Yang, X.: Regularized linear schemes for the molecular beam epitaxy model with slope selection. Appl. Numer. Math. 128, 139–156 (2018)
- Yang, X.: Efficient schemes with unconditionally energy stability for the anisotropic cahn-hilliard equation using the stabilized-scalar augmented variable (s-sav) approach. arXiv preprint arXiv:1804.02619 (2018)
- Zhao, J., Yang, X., Li, J., Wang, Q.: Energy stable numerical schemes for a hydrodynamic model of nematic liquid crystals. SIAM J. Sci. Comput. 38(5), A3264

  –A3290 (2016)
- Zhao, J., Yang, X., Gong, Y., Wang, Q.: A novel linear second order unconditionally energy stable scheme for a hydrodynamic-tensor model of liquid crystals. Comput. Methods Appl. Mech. Eng. 318, 803–825 (2017)
- Zhao, J., Yang, X., Shen, J., Wang, Q.: A decoupled energy stable scheme for a hydrodynamic phase-field model of mixtures of nematic liquid crystals and viscous fluids. J. Comput. Phys. 305, 539–556 (2016)
- 47. Onsager, L.: Reciprocal relations in irreversible processes. i. Phys. Rev. 37(4), 405 (1931)
- 48. Onsager, L.: Reciprocal relations in irreversible processes. ii. Phys. Rev. 38(12), 2265 (1931)
- Qian, T., Wang, X.-P., Sheng, P.: A variational approach to moving contact line hydrodynamics. J. Fluid Mech. 564, 333–360 (2006)
- Xianmin, X., Di, Y., Haijun, Y.: Sharp-interface limits of a phase-field model with a generalized navier slip boundary condition for moving contact lines. J. Fluid Mech. 849, 805–833 (2018)
- Sun, Shouwen, Jing, Xiaobo, Wang, Qi: Error estimates of energy stable numerical schemes for allen–cahn equations with nonlocal constraints. Journal of Scientific Computing, pp. 1–31 (2018)
- 52. Bodewig, E.: Matrix calculus, north, p17 (1959)

Publisher's Note Springer Nature remains neutral with regard to jurisdictional claims in published maps and institutional affiliations.

